2022-07

Influence of matrix and alloying on fatigue crack growth and fracture toughness of compacted graphite iron for cylinder heads

Gonzalez Riquelme, Leny Victoria

UNIVERSIDAD TÉCNICA FEDERICO SANTA MARÍA

DEPARTAMENTO DE INGENIERÍA METALÚRGICA Y DE MATERIALES

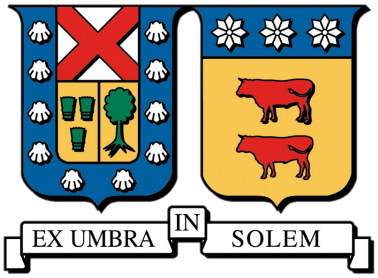

INFLUENCE OF MATRIX AND ALLOYING ON FATIGUE CRACK GROWTH AND FRACTURE TOUGHNESS OF COMPACTED GRAPHITE IRON FOR CYLINDER HEADS

LENY VICTORIA GONZALEZ RIQUELME

Trabajo de memoria de titulación presentado en conformidad a los requisitos y reglamentos requeridos para obtener el título de Ingeniero Civil Metalúrgico

PROFESOR GUÍA: FLAVIO DE BARBIERI

PROFESOR CO-REFERENTE: JUAN DONOSO

PROFESOR CO-REFERENTE: VIKTOR NORMAN

JULIO-2022

Abstract

The continuous modernization of the fuels used demands higher temperatures and pressure in the combustion chamber, consequently the material utilized to manufacture the components involved in the combustion function, such as the cylinder heads, require to improve their properties. The manufacturing company Scania AB® provided seven different compositions samples of compacted graphite iron (CGI) which have been analysed in order to characterize and choose the most suitable material for the serviceability of the cylinder heads. This working report focuses on the impact of the matrix (either pearlitic or ferritic), and alloying elements such as molybdenum and nickel in the fatigue crack growth rate $\left(\frac{da}{dN}\right)$ and fracture toughness (K_{Ic}).

Tests to determine the fatigue crack growth rate, in accordance with ASTM E647 and the fracture toughness (ASTM E399) were carried out. The equipment used was a hydraulics actuator machine, for the fatigue crack growth rate tests and an electro-mechanical machine for the fracture toughness ones. In addition, to measure the length of the crack a portable microscopic camera, an extensometer and a camera connected to a digital image correlation software were used.The processing of the data obtained during the tests was performed with a DIC (digital image correlation) system, TEMA (advanced motion analysis tests software) from IMAGESYSTEMS Ltd. and MATLAB® codes.

Contents

List of Tables

List of Figures

Nomenclature

- ASTM: American Society for Testing and Materials.
- $\frac{da}{dN}$: fatigue crack growth rate.
- TEMA: advance Motion Analysis test software.
- DIC: Digital Image Correlation system.
- LGI: lamellar graphite iron.
- CGI: compacted graphite iron.

Chapter 1

Introduction

1.1 Background

The cylinder head is an essential component for the operation of a vehicle. This is normally located on top of the engine unit. The primary purpose of the cylinder head, as it can be seen in the figure 1.1, is to close the combustion chamber. A further role is to maintain the cylinder lubricated. Otherwise, the engine may not make even a simple movement [1]. Although largely unnoticed, the cylinder head plays a key role in the engine.

The design of the cylinder heads contains three separately different autonomous passages, where cooling fluid and lubricant oil go inside the cylinder. In the meantime, the combustion gases gets expelled. The cylinder design has conducts that allow the cooling fluid to pass by the engine block, which is indispensable to cooling the elements within the engine. To allow the gases and fluids to simultaneously go in or simultaneously to go out of the cylinder, valves are triggered by the camshafts. If the vehicle works with direct combustion the fuel is injected in the cylinder, so the cylinder head shows injectors in its design for this action. The design also prevents oil and water to leak inside the combustion chamber using a head gasket among the cylinder head and the engine block [1].

The main matter found during cylinder head development is the appearance of fatigue cracks during severe endurance tests. These cracks can be initiated in the coolant water jacket, and can be led to the complete part failure [3]. In previous investigations, it was found that microcracks tend to start in the matrix from superficial defects and debonded graphite under cyclic loading at room temperature to 500°C.The cylinder heads are subject to three different types of loads:

1. Static loading due to the tightening on the cylinder block, interference fitting of seats.

2. Thermal loading due to the gas combustion flow, as a consequence of the engine power variation. The loading is cyclic and therefore creates thermo-mechanical stresses under fatigue.

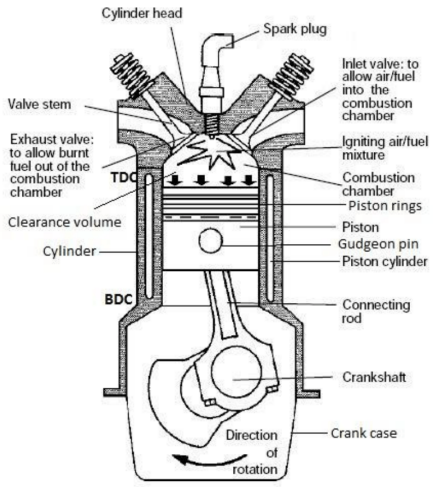

(a) Illustration of a mobile engine parts, including the cylinder head.

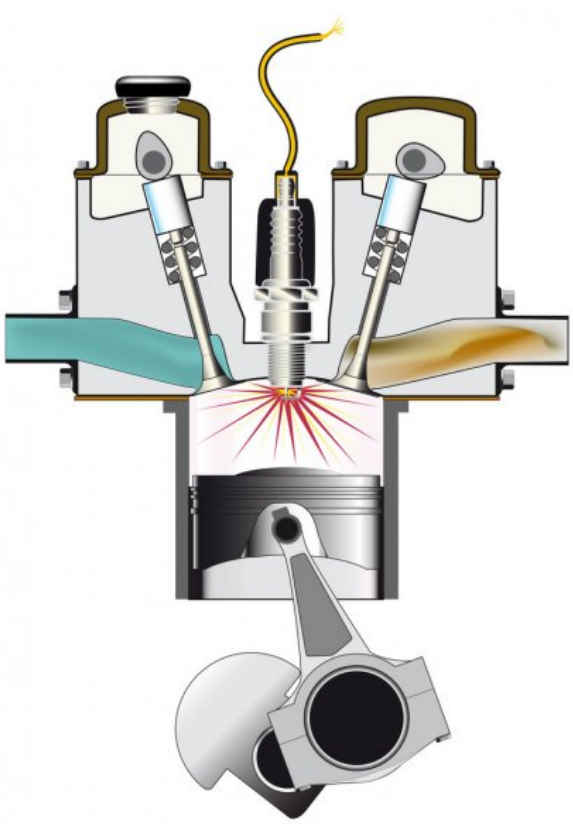

(b) Illustration of a mobile engine.

Figure 1.1: Cylinder heads illustrations [2]

3. Pressure loading at each combustion in the cylinder.

The development of the damage is conditioned by the nature of the material. This encompasses the chemical composition, manufacturing, loading, geometry factor and environment. Therefore, the material and design for a cylinder head should be focused on the fatigue strength properties, considering that their durability is conditioned by them. Nowadays the innovations in combustion processes have been led to an increase in the combustion pressure, this has repercussions in the requirements of the cylinder heads materials properties. The materials normally used for cylinder heads manufacturing are cast irons, which have a high fluidity that allows to fabricate complex shapes [4], they present a high wear resistance and hence more durable and less expensive. Others are made of aluminium alloys which are lighter [5].

The cylinder heads normally can be found made of cast iron, such as lamellar graphite iron (LGI) and compacted graphite iron (CGI) incorporated in a metallic matrix, pearlitic or ferritic [6]. The nature of the chemical composition and the synthesis processes gives the component properties. Thus, the modifications in the chemical composition by adding alloying elements might have a significant effect on the mechanical properties that the material will display at operating

conditions. The type of matrix existing in the material will also define the limits of the mechanical properties.

As explained above, the morphology of the graphite has a large influence in the material properties. In the paperwork "Fracture Toughness and Crack Growth Rate of ferritic and pearlitic Compacted graphite irons at 25%C and 150%C" [7] was found that the fracture toughness values K_{Ic} for an irons with lamellar graphite morphology is between 14-22 MPa$\sqrt{m}$ with a pearlitic matrix, while is in the range of 47.8-61.3 MPa$\sqrt{m}$ for an iron with a compact graphite morphology. Therefore, the variables to be studied are graphite morphology, the alloying elements and the matrix.

The innovation for the cylinder heads' function is required due to the increase in the use of bio fuels, which demands a higher pressure (more detail in 1.2), thereby higher temperature in the combustion chamber. In Europe there was an increase from 180[bar] in 1999 to 220-240 [bar] in 2007 in the pressure in the combustion chamber for vehicles [8]. Compact Graphite Iron fulfills these requirements, doubling the fatigue strength of gray cast iron with a 40% increase in the elastic modulus and around 75% higher ultimate tensile strength [8].

1.2 Purpose of The Study

The global climate is changing, and this is not recent news, therefore measures have been taken to reduce the accelerated impact the planet is suffering. Sweden contemplates, as a pioneer in environmental awareness since many years ago, being the first country to create the Environmental Protection Agency in 1967. Making consecutive conscious decisions over the past fifty years have led Sweden to be one of the most innovative countries in environmental technology, considering the use of smart grids and biofuels [9].

The biofuels are fuels that derive from the processing of biomass through carbon fixation similar to that of plants. The use of plants or animals' substances to generate energy is defined as biomass and therefore biofuels can be generated from industrial, domestic, or agricultural organic wastes and they are, nowadays, a substitute to the consumption of large formation time fuels like that of the fossil ones.

One of the goals for the innovation in the transportation system is to perform a complete change of the biofuels use. The progress in them have developed four generations. The second generation includes the use of biomass to produce fuels (gas or liquid), a technology that has been implemented in Sweden for the past years. Some consequences of the use of biofuels over conventional fuels is that they demand a high efficiency in the combustion. Bio diesel presents some methyl esters with longer carbon chains than the traditional diesel, which displays a higher viscosity that it implies filter plugging issues. For the use of Syngas, which is made from biomass,

the quality is quite lower than natural gas or petrol, due to this, the temperature of the spark ignition (for a spark ignition engine) must be at 30 to 40 Celsius degrees higher than usual [10].

Then, an outcome of the use of biofuels innovation in the engineering of the transportation is needed. For the reason, the cylinder heads' function is exposed to higher temperatures and pressure; thus, a stronger and tougher material is required to be used.

1.3 Effect of the temperature

It is known that the cylinder heads are exposed to high temperatures due to the gas that issues from the combustion chamber. The temperature that the cylinder head material must endure has increased due to the use of biofuels, as it was explained in the section *Purpose of the study* 1.2. It can be expected that high temperatures might have a serious impact on the material component properties. Although, there must be a difference between the temperature of the process inside the cylinder, which can reach 700-900 °C, and the temperature in the cylinder head, this one is no more than 200 °C. On the one hand, it was found in the research "On the correlation between microstructural parameters and the thermo-mechanical fatigue performance of cast iron" [11], that under these cycles conditions 100-500°C the microcracks display a tendency to initiate in microshrinkage porosities instead that in graphite inclusions.

On the other hand, and according to the paper analyzed, "Fracture toughness and crack growth rate for ferritic and pearlitic compacted cast irons at 25 °C and 150°C" [7], it was noticed that the temperature does not affect severely the fracture toughness with values of 1 to 4 MPa$\sqrt{m}$ lower at 150 °C than at 25°C. For the fatigue crack growth rate, increasing the temperature benefits this property by turning it slower. For irons with flake graphite morphology the temperature has a considerable effect. The irons to study contain a medium vermicularity.

1.4 Research questions

1. **How does the chemical composition affect the aspect ratio of the graphite and the mechanical properties of the ferrous alloys studied?**

   The fatigue life is the resistance of a material to undergo cyclic loads having no risk of failure. This project approach is the impact of the material composition in the properties related to the fatigue strength [12]. The fatigue life of the component is influenced by the material properties (chemical composition), design geometry, surface quality, residual stresses, internal defects, grain size, and also some external factors also such as temperature, oxidation, and corrosion. The fatigue strength depends on the factors mentioned above, and the cyclic load to initiate a crack followed by the propagation of it. Even though, the crack

initiation in fatigue occurs commonly at the possible surface defects in the material where the stresses concentrate. This research will consider the influence of the chemical composition, and microstructure (ferritic, pearlitic) in the fatigue crack growth rate ($\frac{da}{dN}$) and fracture toughness of the materials analyzed [12].

2. **What are the advantages and disadvantages of the alloy selected?**

   The influence of the microstructure and the alloying elements in the fracture toughness and fatigue crack growth rate will be studied, aiming to generate a characterization of the impact degree on the material properties. Once the description, for each specimen is done, a comparison between them shows the advantages and disadvantages of the different material alloys. In order to reach a more developed material selection for the cylinder heads. A matrix, ferritic or pearlitic, has specific effects on the material properties as well. On the one hand, a ferritic matrix allows a percent of ductility, but lacks mechanical strength. On the other hand, a pearlitic matrix gives a higher mechanical strength and hardness to the material [13].

   The percentage of alloy elements in the material composition can impact the fracture toughness either positively or negatively, depending on the effect that they have on the graphite and the matrix phases. The awareness of the advantages and disadvantages of the alloy selected is indispensable, since they state the component performance at the service conditions.

1.5 Hypothesis

The hypothesis to affirm or refuse is:

The combination of a ductile matrix, such as the ferritic, with the effect of the alloying elements on the graphite will give an improved alloy in terms of fracture toughness and fatigue crack growth rate in comparison with the pearlitic specimens for the different alloys composition to test and reported values considered.

1.6 Objectives

In order to approve the hypothesis presented and make this research possible is to be required to establish the general and specific objectives that will give a direction to it.

- **General objective**

  1. From the set of alloys to test, select the alloy that permits the highest fracture toughness, evaluate the fatigue crack growth rate and compare with the reported values.

Since the material requirements have changed, expecting longer durability to higher temperature and pressure, the alloy that displays the highest value of fracture toughness will have a better resistance to these service conditions.

In order to guarantee a good performance of the material under fatigue conditions, from the perspective of tests environment, is important to consider the properties involved, such us fracture toughness and fatigue crack growth rate. The component performance, in this case a cylinder head, includes another aspect besides the material properties, this one is the manufacture of the component. Superficial defects and stress concentrator can easily initiate a crack.

- **Specific objectives**

1. Analyze the influence of the matrix, pearlitic or ferritic in the fracture toughness and fatigue crack growth rate properties.

   In recognition of the results of the research *Fracture Toughness and Crack Growth Rate of ferritic and pearlitic Compacted graphite irons* [7] it is possible to obtain higher values of fracture toughness for a pearlitic matrix. This does not decline the option of getting a better performance for a sample with a ferritic matrix and alloying elements, such as nickel and molybdenum.

2. Analyze the effect and correlation of the quantity and type of alloying elements on the hardness, aspect ratio of the graphite and the properties of fracture toughness and fatigue crack growth rate of the alloys to be tested.

   The material properties are directly related to the chemical composition and synthesis processes to achieve the component. To get reliable results it is relevant to follow the ASTM standards since they have a precise and complete method to obtaining and validating the values of fracture toughness and fatigue crack growth rate tests.

   ASTM develops different standards to apply for material testing. In this occasion two ASTM standards are followed, E399 and E647. The fatigue crack growth rate test is performed guided by the standard E647, which presents the method to measure the fatigue crack growth rate [14]. The fracture toughness test follows the standard E399, that corresponds to the test method for plane-strain fracture toughness of metallic materials [15].

Chapter 2

Literature review

2.1 Classification of cast irons

In the wide field of metal alloys these can be classified in two types, ferrous and non-ferrous. The ferrous alloys have many sub-group classifications as can be shown in the figure 2.1. The main difference between steel and cast iron relies on the carbon content. The steel contains between 0.1-0.5 % of carbon, while a cast iron is compound from a range of 2-4 % of carbon, this last amount gives peculiar characteristics such as low liquidus temperature and high cast fluidity [4].

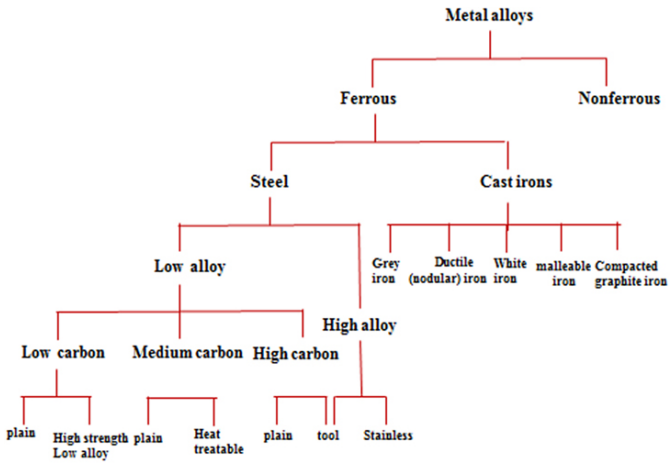

Figure 2.1: Classification of Metal Alloys from Concepts in Physical Metallurgy. [16]

Cast irons can be categorized as white, gray, nodular (spheroidal) and compact cast iron. The first one presents the carbon as iron carbide plates (Fe_3C with 6,67% C) and a gray dull crystalline fracture surface. Meanwhile, the gray iron (also named lamellar graphite iron) exhibits the carbon as graphite (which contains 95-99 % of carbon) in the shape of flakes with a gray fracture surface [17]. A nodular graphite iron - also named spheroidal graphite iron - presents the graphite in

spheroidal morphology. Finally, in the compact graphite iron (CGI)- there is a combination of worm shaped with round edges graphite and nodules [18].

The high fluidity of the cast iron permits to achieve different and complex types of shapes for the final product, which amplify the uses given to them. Even though, they are highly brittle and display a tendency to get rusty. They also have a great wear and deformation resistance [17].

2.1.1 Vermicularity

For a better comprehension of the graphite morphology in the specimens for this project, the vermicularity concept will be introduced.A vermicular morphology corresponds to a graphite with the shape similar to a worm. The vermicularity concerns the percent of vermicular morphology observed in the specimen graphite [7]. Therefore, the nodular cast iron has a very low or no vermicularity. In contrast, the gray cast iron will have a high vermicularity. The compact cast iron is expected to have a medium vermicularity morphology. A low vermicularity refers to a nodule morphology, which is a round similar to spheroidal shape of graphite, while a high vermicularity can be associated to a flake graphite morphology.

2.2 Matrix types

The type of matrix to achieve will depend on the chemical composition, solidification rate and heat treatments [4]

- Ferritic The graphite is incorporated in a matrix which can be ferritic or pearlitic. The ferrite is a phase characterized for being soft, ductile and for having a low carbon solubility, around 0.008 % at room temperature and 0.022% at 727° C.
- Pearlitic The pearlitic phase is compound of layers of ferrite and cementite. Therefore, its properties are brittle and hard due to the high amount of carbon (6.67% C) in the cementite. In contrast, the ferrite layers are ductile and soft.

The effect of the microstructure is a relevant analysis. The amount of graphite in it can signify more possibilities for the crack to propagate through the brittle graphite [19]. Furthermore, a ferritic matrix can help to dissipate the stress the specimen experiments being under fatigue conditions since it is more ductile. Otherwise, the strength might not be high enough for the conditions and will lead the specimen to failure. The cementite layers found in the pearlitic matrix can have an important contribution to the iron strength and hardness, increasing the fatigue life of the component [19].

2.3 Graphite Morphology

The properties of the cast irons are given by the chemical composition. Therefore, the alloying elements are a relevant parameter. The alloying element that is essential for cast irons is the silicon (Si), since it has the effect of maintaining the carbon out as a second phase forming the graphite. The amount of silicon can vary between 1-4 % [17].

The mechanical properties are linked to the chemical composition and microstructure of the material. The aspects related to the microstructure of the material include the graphite morphology, which can be presented as nodular (low vermicularity), compact (medium vermicularity) or vermicular (high vermicularity), see figure 2.2. The impact of flake or vermicular morphology displays an important aspect. They act as stress concentration areas, turning the flakes in an unwanted graphite morphology. Therefore, a more elongated graphite (flake) will generate a higher crack growth rate. It has also been found that the elastic modulus of cast irons is associated to the graphite morphology. Additionally, the yield strength and ultimate tensile strength are influenced by the type of matrix and graphite morphology [11].

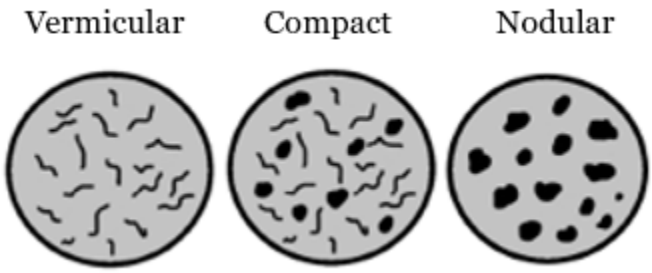

Figure 2.2: Different graphite morphologies for cast irons.

The lamellar graphite iron exhibits a low ultimate tensile strength due to the graphite flakes (UTS strength 110.9 – 134.7 [MPa]) [7], at compression the strength can reach higher values, near the double than in tension. A nodular morphology will allow the material to distribute the stress increasing the strength (UTS strength 389.6 – 532.5 [MPa]) [7]. The compact graphite iron presents an intermediate vermicularity, it is not as low as the nodular cast iron or as high as the gray cast iron (UTS strength 257.6 – 367.8 [MPa]) [7].

If a comparison is made between lamellar graphite iron (LGI) and compacted graphite iron (CGI), this last one has higher fracture toughness, (K_{Ic} 47.8 – 56.3 [MPa$\sqrt{m}$] for CGI and for LGI K_{Ic} 14.4 - 22.0 [MPa$\sqrt{m}$])[7]. Furthermore, the properties of the CGI are less dependent on the specimen geometry than the LGI. On the other side, some benefits of CGI over the nodular graphite iron are that has a lower thermal expansion coefficient, a lower level of stress thermally induced which gives the CGI superior thermoshock resistance along with improving damping capacity,

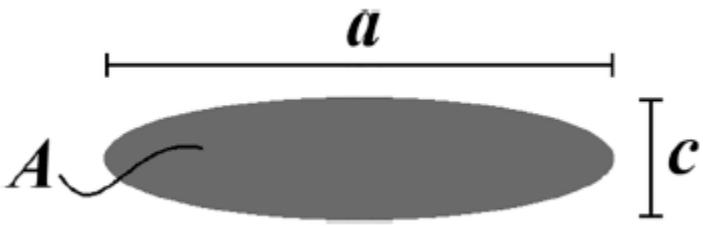

Figure 2.3: Diagram of a graphite inclusion considering its length, a, width, c and area, A [11].

pouring properties as shrinkage, mold-filling and fluidity [18].

It is important to understand the dimensions involved in a graphite inclusion, as it can be seen in the figure 2.3 a corresponds to the length of the graphite inclusion diagram, c is the width and A the area of it. Further $\frac{a}{c}$ represents the aspect ratio of the graphite, and its correlation on the fatigue properties will be analyzed.

2.4 Fatigue

The phenomenon of fatigue condition refers to a progressive, localized and permanent structural change that can occur in materials under fluctuating loads [12]. The strains produced, due to these loads, might cause the growth of cracks which can culminate in the material failure after a certain amount of cycles. For the initial crack to propagate under fatigue conditions some requirements must be considered. The crack can be initiated from a surface defect or stress concentration area of the material in combination with the cyclic stresses [12].

The fatigue fracture has three stages according to the fatigue testing [20]:

1. First, initial defects can work as crack nucleation and initiation.
2. Second, the crack growths macroscopically until a critical magnitude in comparison with the section of the material uncracked.
3. Third, the component reaches abrupt failure.

The cyclic stresses for the fatigue cracking are considerably lower than the static yield strength of the materials[12]. Therefore, it is relevant to study the fatigue behavior of materials exposed to cyclic loads conditions.

2.4.1 Cyclic Loads

The cyclic loads are defined as the variable loads from one peak to another: see figure 2.4. Cyclic loads can not be found in the nature, but can be easily exemplify and understood by the passing of

a train or truck over a bridge [21]. In a general case the cycles do not have the same amplitude[22], such as the train, truck, or cars passing over a bridge since they have different mass. They induce different loads. For a component application under fatigue, it is expected that the cyclic loads vary in a systematic manner during the operational life of the component [23].

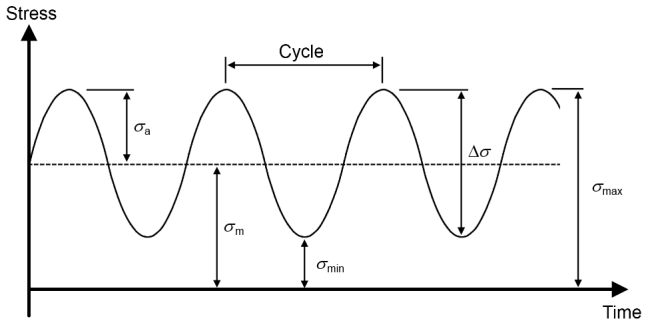

Figure 2.4: Description of cyclic parameters [22].

In the figure 2.4 σ_a represents the amplitude of the stress. This is defined by the equation below 2.1, which is usually measured in [MPa].

$$\sigma_a = \frac{\sigma_{max} - \sigma_{min}}{2} \tag{2.1}$$

Where:

σ_a : the stress amplitude [MPa].

σ_{max} : the maximum stress in a cycle [MPa].

σ_{min} : the minimum stress in a cycle [MPa].

The minimum stress in the cycle is σ_{min} and the σ_{max} the maximum stress. Additionally σ_m corresponds to the mean stress which is defined as the following equation 2.2.

$$\sigma_m = \frac{\sigma_{max} + \sigma_{min}}{2} \tag{2.2}$$

The stress range $\Delta\sigma$ is expressed as $\Delta\sigma = \sigma_{max} - \sigma_{min}$. In this figure it is clearly possible to observe the parameters of a cycle as the variation between two stress peaks.

The effect of the cyclic loads in the fatigue strength of the material will depend on the frequency, the main stress and the stress amplitude of the load applied [22].For example, the effect of cyclic loads at high frequency might have severe impact on corrosive environments[24].

2.5 Stress Intensity Factor *K*

Due to the high level of stress that the head cylinder needs to bear under fatigue condition, the concept Stress Intensity Factor (K) becomes relevant. The stress intensity factor describes

the stress level around a crap tip or a notch. This value is used in fatigue conditions to obtain information regarding the critical stress which leads to an accelerated crack growth that culminates in fracture. The stress intensity factor (K) depends on the specimen geometry, and it is measured in MPa $\sqrt{m}$ [25].

The theory behind the stress intensity factor is to be explained by understanding the demeanor of a specimen that is pre-cracked and under a specific load. The higher the load applied, the higher the stress experimented by the specimen and vice versa. Thereby, if the load applied is too high, so the K will be, leading the specimen to a very high stress level that can make it collapse. The crack will propagate through the specimen generating a fracture failure. In contrast, there is a small load that permits the specimen to endure infinite time without experimenting plastic deformation at this condition [26]. Professor Paul Croce Paris postulated that the stress intensity factor works as a function of the stress and the crack length in the specimen [26]. The stress intensity factor is found to control the dynamic fatigue crack growth as well as the static fracture and environmental assisted cracking[26].

There are three modes of stress intensity presented in the figure below 2.5. The first, K_I, will be used in the tests procedure and it indicates the fundamental tensile model loading [27].

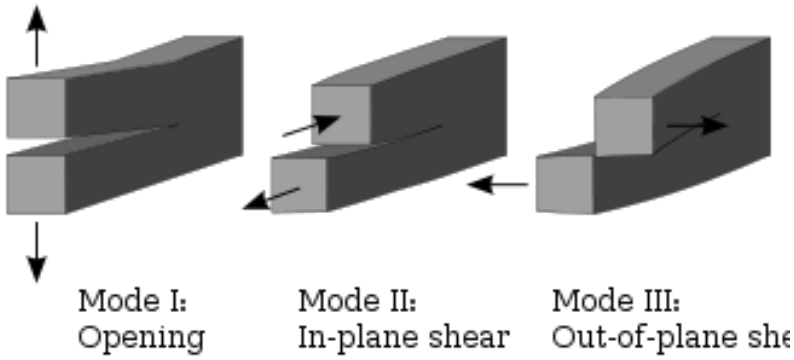

Figure 2.5: Fracture modes [28].

2.5.1 Stress Intensity Factor Range ΔK

In cyclic loading the stress applied is going to be described as sinusoidal, thus the stress intensity factor is going to have a maximum and minimum value see equation 2.3. Therefore, the Stress Intensity Factor Range is the difference between the maximum stress intensity factor in a cycle and the minimum stress intensity factor in a cycle [14].

$$\Delta K = K_{max} - K_{min} \tag{2.3}$$

Where:
K_{max} : the maximum stress intensity value in a cycle [MPa$\sqrt{m}$].
K_{min} : the minimum stress intensity value in a cycle [MPa$\sqrt{m}$].

2.5.2 Plane-strain fracture toughness K_{Ic}

The denotation K_{Ic} corresponds to the fracture toughness property and it describes the crack extension resistance under the mode I mentioned in the stress intensity section 2.5. It is a measure of the crack growth resistance from the initial crack (extension of 2% or less) under slow rates of loading, mainly in linear- elastic conditions (plane-strain)[12] [29].

2.5.3 Effective Stress Intensity Factor ΔK_{eff}

Occasionally, when an external load is being applied to the specimen during a cycle, the crack might not open. In this case, it is necessary to reach a certain opening stress (K_{op}). From this opening stress value to the maximum stress value (K_{max}), the crack will be open by an increase of the load, see figure 2.6 [26]. This phenomenon is called *crack closure* and it can occur due to plastic deformation, phase transformation during the crack growth, fluids or corrosion in the crack surfaces [30]. Therefore, the Effective Stress Intensity Factor ΔK_{eff} can define the range where the crack opens, its mathematical expression corresponds to the difference between the maximum stress intensity factor and the opening stress intensity factor, see equation 2.4.

$$\Delta K_{eff} = K_{max} - K_{op} \tag{2.4}$$

Where:
ΔK_{eff} : effective stress intensity factor [MPa$\sqrt{m}$].
K_{max} : the maximum stress intensity value in a cycle [MPa$\sqrt{m}$].
K_{op} : the opening stress intensity value in a cycle [MPa$\sqrt{m}$].

2.6 Fatigue Crack Growth Rate

It is the change of the crack size with the number of cycles, these values are measure at a certain crack size ($\frac{da}{dN}$) [31] and corresponds to the slope at each point of the figure 2.8.

The fatigue crack growth rate is not constant during all the specimen fatigue life, see figure 2.7. It is predictable that in the first stage, the rate is going to be slow. Then, in the second stage the curve will have a lineal demeanor which can be described by the Paris' law expression,

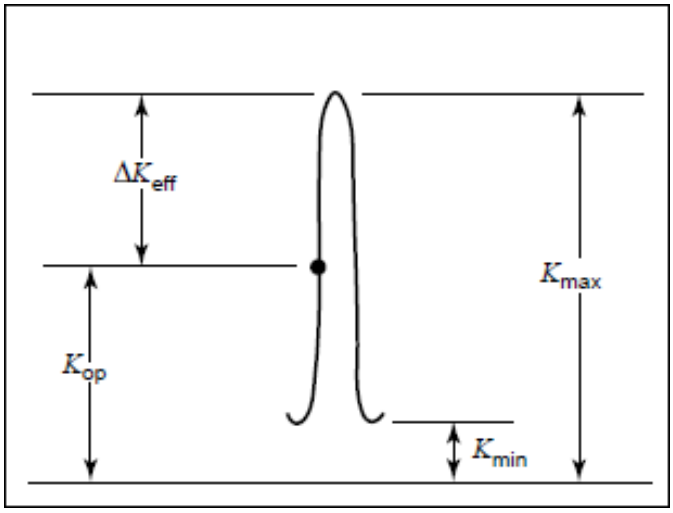

Figure 2.6: Stresses involve in crack surface opening [26].

see equation 2.5. The last stage, it is characterized for having a rapid and unstable growth until fracture [32].

In the middle region of the crack growth rate curve versus the stress intensity range in logarithmic scale (see figure 2.7), the fatigue crack growth rate will be controlled mainly by the stress intensity factor, with a small influence of other aspects [32]. In the first region the factors that influence largely are: the microstructure, the mean stress and the environment. While during the final region, the aspects that influence the crack growth are: the microstructure, the mean stress and the thickness of the component [31].

$$\frac{da}{dN} = C(\Delta K)^m \tag{2.5}$$

Where:

$\frac{da}{dN}$: crack growth rate [m/cycles].

C and m : materials constants for crack growth, C in $\left(\frac{\frac{m}{cycle}}{(MPa\sqrt{m})^3}\right)$ [1] and m is dimensionless.

ΔK : stress intensity factor range [MPa$\sqrt{m}$].

The stresses (residual, cyclic loads and thermal stresses) experimented by the component or specimen in the case of the laboratory work, along with the material properties such as fatigue strength properties, will define the rate of growth of a crack.

2.6.1 Fatigue crack growth rate relation with stress and Crack length

In order to obtain the crack growth rate, the crack length data during the fatigue test must be acquired. This can be done by the use of compliance or electric potential difference method.

[1] For simplify and avoiding confusion with the units, the power of 3 corresponds to m=3.

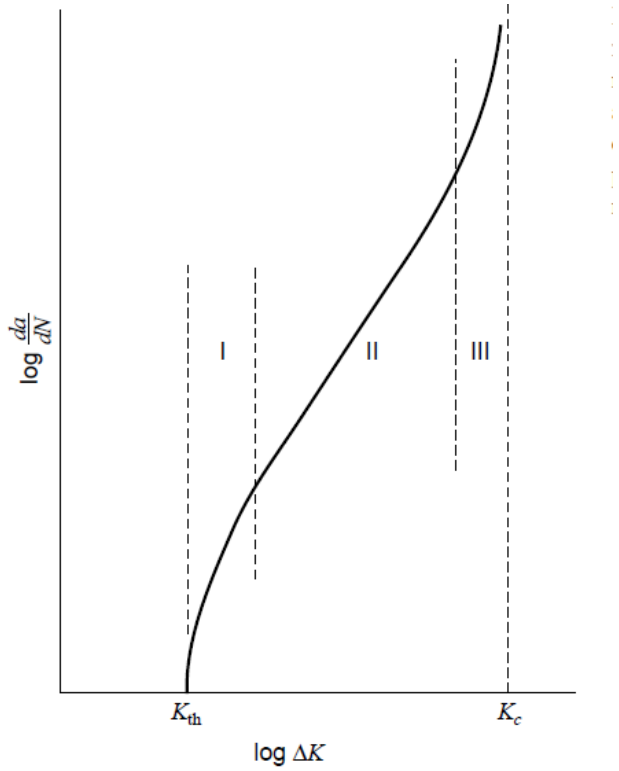

Figure 2.7: Crack growth stages [26].

Consequently, tests have been performed by fatigue researchers, in which it has been observed, for almost all the cases, that the fatigue crack growth rate increases proportionally with the crack length. Another important relation is that the fatigue crack growth rate rate has a relevant magnitude correlation with the stress applied as can be noticed in the figure below 2.8. Where a higher stress leads the component to endure less number of cycles (N) and a minor crack length (a) until the material breaks [26].

As it is described in the chapter 10 of the book Deformation and fracture mechanics [26]. During the 60's decade, several experiments were performed with the aim of understanding the demeanor of the fatigue crack growth rate.

2.6.2 Fatigue Crack Growth Threshold ΔK_{th}

Through the curve of the fatigue crack growth rate a threshold regime can be defined. According to the ASTM Standard E647 [14] the ΔK_{th} correspond to the value at which the fatigue crack growth rate approaches to zero, see figure 2.7. For almost all materials the value of ΔK_{th} is given at a fatigue crack growth rate of 10^{-10} m/cycle.

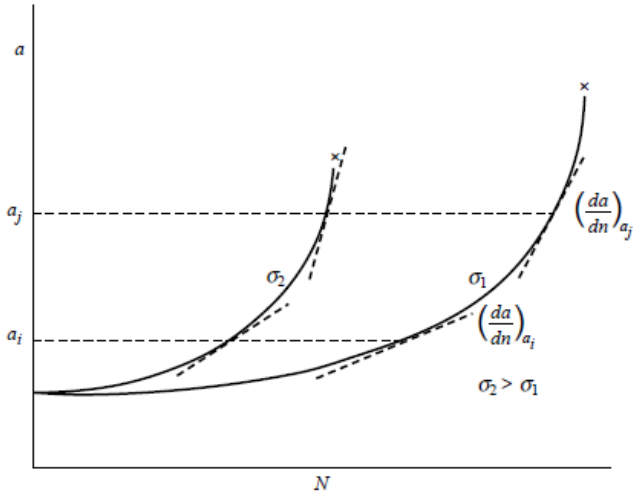

Figure 2.8: Stress effect on the fatigue crack growth rate from Deformation and fracture mechanics of engineering chapter 10 [26]

2.6.3 Plane-strain condition

The fracture toughness test performed in this research follows the standard for plane strain fracture toughness of metallic materials (E399) [15]. The fatigue fracture has three stages [26]. In the first stage the crack will have a 45° with the xy plane in reference to the loading direction. Thereafter, it will change to the loading direction allowing the crack to propagate. During the second stage, the plane of the crack growth will depend on the stress level the specimen endures. In the section stress intensity factor 2.5, the relation of how the stress applied influences the intensity that the specimen experiences was established. Therefore, a small stress intensity factor range produces a small plastic deformed zone. Yet, a big plastic deformed zone will generate at high ΔK values. A plane strain condition is accomplished when the thickness of the specimen is large in comparison with the plastic zone size giving a flat fracture. When the plastic zone size is larger than the specimen thickness, a plane stress condition takes over the fracture, and an incline fracture is developed [26].

2.7 Influence of the type of matrix and vermicularity on the fracture toughness and fatigue crack growth rate

The fracture toughness (K_{Ic}) and fatigue crack growth rate properties have been studied for cast irons with pearlitic and ferritic matrices and for different grades of vermicularity (for further understanding of this concept, take a look at the subsection 2.1.1). The values obtained for the fracture toughness and fatigue crack growth rate according to the research "Fracture Toughness

Microstructure		Temperature 25°C		
Matrix	Vermicularity	K_{Ic}[MPa$\sqrt{m}$]	m	C
F	10 %	54.5	4.51	$5.1 \cdot 10^{-13}$
	50 %	47.8	4.60	$1.6 \cdot 10^{-13}$
	90 %	43.0	9.97	$5.8 \cdot 10^{-21}$
	Flakes	14.4	12.98	$7.9 \cdot 10^{-23}$
P	10 %	69.6	5.04	$6.9 \cdot 10^{-13}$
	50 %	61.3	7.02	$7.9 \cdot 10^{-18}$
	90 %	56.3	11.79	$2.2 \cdot 10^{-22}$
	Flakes	22.0	17.80	$1.5 \cdot 10^{-32}$

Table 2.1: Values of fracture toughness and Paris' law constants for different types of matrices and vermicularity for cast irons.

and Crack Growth Rate of ferritic and pearlitic Compacted graphite irons at 25%C and 150%C" [7] can be seen in the table below 2.1.

Taking these values in consideration, it can be noticed that there is an increase of 14-17 [MPa$\sqrt{m}$] for the fracture toughness when changing the matrix from ferrite to pearlite. This trend is noticed throughout the range of vermicularity. The reason for this tendency could be due to the ferrite and cementite layers that are contained in the pearlite matrix. The cementite has a 6.67% of carbon which deforms the lattice structure producing an increase in the hardness of the material. The combination of ductile ferrite layers and hard layers as cementite causes a considerable increase in the fracture toughness of the alloy. For the alloys to test in this research, it is expected to get values within 30-40 [MPa$\sqrt{m}$], which are near the fracture toughness of 90% vermicularity samples. The information regarding to the level of vermicularity of the samples to be tested is not exactly known, since the providers have noticed that the alloys correspond to compact graphite iron, which means that a relevant percentage of vermicularity in its composition could be observed.

The material constants C and m are related to the second region of the differential curve of the crack length and the number of cycles in logarithm scale, also known as *Paris' Law*, a further explanation of the theory that sustain this concept can be seen in the section 2.6. In the information related to the paper, it was seen that the ferritic matrix specimens present a trend to display smaller m values, thus, a slower fatigue crack growth rate was identified in comparison with the samples with a pearlitic matrix. This can be due to the ductility of the ferritic phase facilitating the crack blunting mechanism to occur.

In the table 2.2 can be seen the m and C values for different types of alloys. Taking this data into consideration, it is expected that the values to obtain for the m constant would be over 3 and under 8, since the compacted graphite irons with a vermicularity of 50-90 % tend to display a bigger m values comparing to steel. For the C constant is expected that the values might be

within the range of 10^{-13} to 10^{-18} considering the 50% and 90% vermicularity in the table 2.1. Moreover, it must be taken into account that nickel is found in some of the specimens to test as an alloy element. Even though, the grade of vermicularity in the alloys is not known, it is reasonable to consider that their vermicularity is within the range of 50-90%.

Alloy	m	C
Steel	3	10^{-11}
Aluminum	3	10^{-12}
Nickel	3.3	$4 \cdot 10^{-12}$
Titanium	5	10^{-11}

Table 2.2: Table with C and m values for the regimen of the Paris' Law for different alloys [33].

2.8 Influence of molybdenum and nickel on the aspect ratio and by extension the alloy properties

On the one hand, to increase the hardness and strength of the material the molybdenum is added in quantities of 0.3-1 % in pearlitic cast iron [34]. These improvements can be done because of the decrease in the temperature for the pearlite transformation [35]. The molybdenum has a strong effect of refinement over the graphite flakes [36]; it also reduces the inter layers space of the ferrite and cementite in the pearlitic matrix which means a strength increase [34].

On the other hand, nickel is added to the composition of cast irons for the graphitizing effect. In other words, it promotes the graphite formation, and it has a refinement effect on it. However, it is not as strong as the molybdenum [36]. The pearlite refinement improves the strength and hardness of the material.

2.9 ASTM Standards

The American Society for Testing and Materials is an organization that develops and provides standards for materials, products, services and systems worldwide [37]. In this research the ASTM standards E 399 and E 647 are used to carry out the fracture toughness and fatigue crack growth rate tests respectively.

Chapter 3

Methodology

3.1 Relevant terminology

1. Crack size (a)

   It is the lineal dimension of the crack and it is measured in millimeters [mm] [12]. The crack size is used for fracture mechanics parameters such us fatigue crack growth rate.

2. Force range (ΔP)

   Represents the difference of consecutive valley and peak forces, defined as positive, and negative for the difference between successive peak to valley [12].

   $$\Delta P = P_{max} - P_{min} \tag{3.1}$$

   Where:

   P_{max} : maximum force applied in a cycle.

   P_{min} : minimum force applied in a cycle.

3. Stress ratio (R)

   It is the ratio between the minimum force and the maximum force applied in a cycle [12].

   $$R = \frac{P_{min}}{P_{max}} \tag{3.2}$$

3.2 Focus of the Methodology

There are different ways of approaching the nature of a problem. For instance, gaining more understanding of it might be not only describing the characteristics of a topic, but through the focus of the cause and effect as well. This research involves both means to approach the problem studied.

It is also important to define the sort of data to work with. In this situation, quantitative data from the tests performed is used. The kind of analysis to apply from the obtained data will be between groups for the different types of matrices, and within groups to evaluate the influence of the weight percentage of alloying elements.

3.3 Description of the method

For a further comprehension of the work to perform, see the diagram below 3.1.

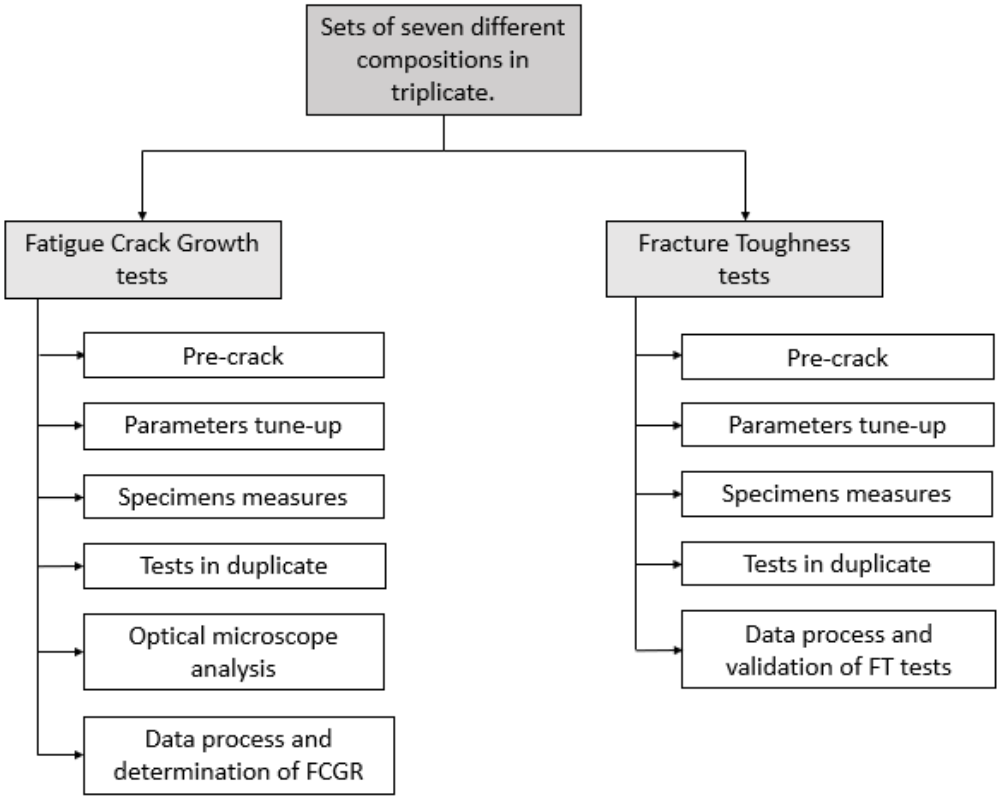

Figure 3.1: Diagram with the methodology for the performance of fracture toughness and fatigue crack growth rate.

- There are two sets of seven different compositions of samples in triplicate to analyze. The specimens compositions are displayed in the table 3.1. The complete chemical composition

Matrix	Denotation	Composition		
		%Mo	%Ni	%Si
Perlitic	1MM RC	0.05	0.05	2.30
	4MM	0.25	0.05	
	10MM	0.05	0.50	
	16MM	0.05	1.00	
Ferritic	20MM RC	0.05	0.05	4.00
	26MM	0.15	0.05	
	36MM	0.25	0.05	

Table 3.1: Table with specimens denotation and chemical composition.

is in the table 6.1. One round of specimens will be left out of the tests to be used in case a specimen fails. The specimens named only as ferritic and pearlitic correspond to the ones with a reference composition. The dimensions for both types of specimens, C(T) and bend configuration, can be observed in the table 3.2.

Specimen dimensions	C(T) [mm]	Bend [mm]
W	25	18
B	12.5	9.08
a_o	10	6.99

Table 3.2: Dimensions: W (width), B (specimen thickness), a_o (original crack size) for C(T) and bend specimens.

The **MM** denotation in the first column of the table 3.1 means medium solidification rate and medium cooling rate.[1]

- Two types of tests are performed, fracture toughness according the standard E399 and fatigue crack growth rate following the standard E647.
- For both types of tests, two rounds of experiments are performed to all the compositions. It is essential to remark that for the fracture toughness test the specimens need to be pre-cracked.
- Independent variables: Matrix (pearlitic or ferritic) and alloying elements Ni in 0.5% and 1 %, Mo in 0.25% and 0.5%.
- Dependant variables: graphite morphology, fracture toughness (K_{Ic}), fatigue crack growth rate $\left(\frac{da}{dN}\right)$, Paris' law parameters, C and m.
- For both types of tests (fracture toughness and fatigue crack growth rate) dummies specimens were used to tune up the parameters.

[1]RC: 0.05% Mo 0.05% Ni

3.4 Justification of the methodology

The execution of the methodology presented allows to acquire reliable data from the tests to perform and to obtain an integral characterization of the alloy selected due to its response to the tests. The results will provide an understanding of the influence of the composition (considering the alloying elements and their quantities), and microstructure on the mechanical properties of the selected alloy. Furthermore, an analysis for relating the graphite aspect ratio, and the hardness with the fatigue crack growth rate, and the fracture toughness of the materials, is performed through the information provided from two other research groups that analysed the same specimens compositions. Their investigations are, *The casting procedure's impact on the microstructure* [38] and *The importance of the microstructure for the mechanical properties of compact graphite iron* [39].

3.5 Fatigue crack growth rate test

For performing the fatigue crack growth rate tests, the standard ASTM E647 is followed.

3.5.1 Standard Test Method for Measurement of fatigue crack growth rates, ASTM E647.

This standard contains detailed information of the steps to carry on tests, as well as calculations and analysis of the data. A fatigue crack growth rate test is performed under the linear elasticity demeanour of the material for the applied force. This method, the standard ASTM E647, is applied to pre-cracked notched specimens.

The results are expressed in $\frac{da}{dN}$ vs ΔK, so the existing outcomes are independent of the specimen planar geometry.

The tests are developed in an inert environment, in other words, no high temperatures or corrosion and oxidation risk. Due to this condition, the fatigue crack growth is expected to be characterized as a function of the stress intensity factor range (ΔK) and the stress ratio (R) [14].

The procedure followed was the K-increasing test, since it has less variability. This type of test is suitable for rates over 10^{-8} m/cycle, under this value of rate the fatigue crack growth is sensitive to small variations in the stress intensity range. It is also recommended to perform the test at constant force amplitude for rates above 10^{-8} m/cycle to avoid transient rates, product of changes in the P_{min} or the stress ratio [14].

In the section 9 of the standard E647, *calculation and interpretation of results* [14], it is advised to calculate a crack curvature correction factor(CCC) to consider the difference between the physical and the software crack measures.

The specimen dimensions can be observed in the figure 3.2, where W corresponds to the width of the specimen. The dimensions fulfill the standard annex A1 for a C(T) configuration [14].

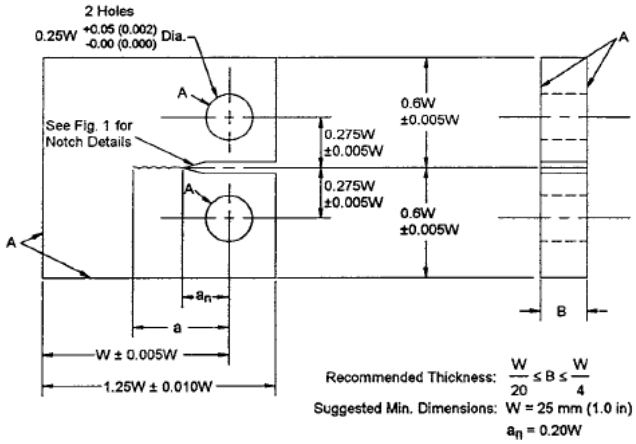

Figure 3.2: Specimen configuration (C(T)), for the fatigue crack growth rate test.

3.5.2 Fatigue crack growth rate test features

The aim of this test is developed to obtain data representing the real fatigue crack growth demeanour of the materials analyzed. There are seven different compositions, compound by three specimens each, which were numbered: N°1, N°2 and N°3. The fatigue crack growth test was performed in duplicate to consider the variability of the method. Therefore, the specimens N°1 and N°2 were tested, N°3 were kept in case of need.

3.5.3 Fatigue crack growth rate data acquisition equipment

A Mini MTS Bionix® 858 machine is utilized for the test which works with servo hydraulic systems. This means that a servo valve will receive the hydraulic fluid that comes from a hydraulic pressurized cylinder [40], see figure 3.3a. The machine has an axial and torsional limit of 25 [kN][41]. The data acquisition was obtained through the use of a clip-on extensometer, located in the sharp edges of the C(T) specimens. The software named Doli was utilized, which has a special interface for performing fatigue tests. The crack length is measured previously to start the tests (apart from the software crack length data). For this, a vernier caliper is used, and it is compared with the measure obtained from the photos took using a DIC (Digital image correlation) equipment. A DIC system is a 3D and non contact optical technology for measuring contour, deformation, vibration and strain. This technique of measuring is commonly used for mechanical and material testing, its versatility allows to utilized this equipment for dynamic or Static testing, including tensile, torsion, bending and combined loading.

The DIC system works with a camera (see figure 3.3b) connected to a computer with a software named TEMA. The latter is used for advanced motion analysis tests. This software has several tools for non-contact optical analysis on specimen surfaces considering strain and displacement. Within the tools, it is allowed to take measures of the specimen of the crack size (initial, during and final crack size) with a better precision over the human eye. Also, the TEMA and DIC system were essentially used for obtaining the displacement in the fracture toughness tests, see subsection 3.6.3.

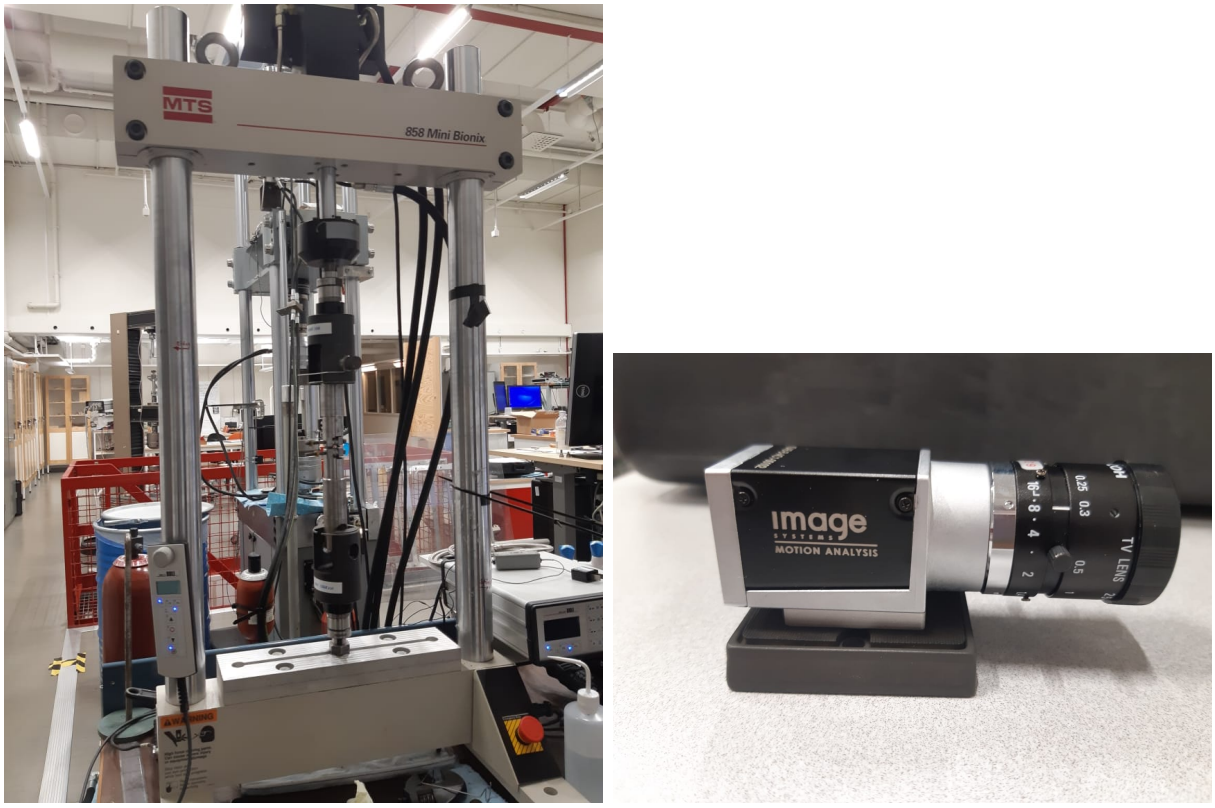

(a) Mini Bionix 858 machine used for the fatigue crack growth rate tests.

(b) DIC system camera used to take measures with the software TEMA.

Figure 3.3: Fatigue crack growth tests equipment.

3.5.4 Fatigue crack growth rate data acquisition method

The extensometer measures the crack opening during the experiments which is connected to the software Doli. Through the compliance method is possible to calculate the crack length as it is indicated in the annex corresponding to the C(T) specimen [14]. Here is the equation that shows the mathematical expression to calculate the crack length 3.3.

$$\frac{a}{W} = c_0 \ + \ c_1 \cdot u \ + \ c_2 \cdot u^2 \ + \ c_3 \cdot u^3 \ + \ c_4 \cdot u^4 \ + \ c_5 \cdot u^5 \tag{3.3}$$

$$u = \frac{1}{\sqrt{B \cdot E \cdot \frac{v}{P} + 1}} \tag{3.4}$$

Where:

c: Constants that depend on the extensometer position.

a: crack length.

W: specimen width.

B: specimen thickness.

E: elastic modulus.

v: crack opening displacement.

P: load.

It is important to remark that the dimension- width, thickness and notch length (initial crack length)- of each specimen is measured with a vernier caliper before performing the tests. For calculating the stress intensity (K) the software uses the expression below 3.5.

$$K = \frac{P}{B \cdot W^{0.5}} \cdot f(d) \tag{3.5}$$

$$f\left(\frac{a}{W}\right) = f(d) = \frac{2+d}{(1-d)^{1.5}} \cdot (0.886 \ + \ 4.64 \cdot d \ - \ 13.32 \cdot d^2 \ + \ 14.72 \cdot d^3 \ - \ 5.6 \cdot d^4) \tag{3.6}$$

Where:

K: stress intensity factor.

P: load.

The stress intensity factor range (ΔK) is calculated by multiplying the K for the difference of one minus the stress ratio (R).

$$\Delta K = K_{max} \cdot (1 - R) \tag{3.7}$$

Doli software parameters

The input parameters for the fatigue crack growth rate tests can be seen in the following table [2] 3.3.

[2]The elastic modulus shown as a parameter in the table is a reference value. The real values, for the specimen tested, were obtained once the fatigue crack growth rate tests were already performed. Another research group were in charge of obtaining these results, for further information see [39].

Parameter	Value	Units
Maximum force	4000	[N]
Minimum force	200	[N]
Stress ratio	0.05	[-]
Frequency	10	[Hz]
Elastic modulus	150	[GPa]

Table 3.3: Established parameters for the fatigue crack growth rate tests.

3.5.5 Leica Optical Microscope Crack Photos

Once all the tests being performed for fatigue crack growth rate, the specimens N°2 will be polished with the silicon carbon grinding papers # 220, # 500, # 1200 and # 4000. The aim of the microscope images is to compare the final crack length that the software Doli indicates with the crack length measured through the vernier caliper and with the microscope software. This procedure will allow to make a posterior analysis to validate the values of the crack length.

3.5.6 Data interpretation

A software called MATLAB® will be used for analysing the data obtained, since the Doli software does not allow to continue the same test once it is stopped to take measures a *"new test"* is needed to be done. By using MATLAB® , the several test parts (between 4-5) can be merged, so after the data being analysed for the specimen tested. As a result, the fatigue crack growth rate charts can be plotted in a logarithmic scale.

3.6 Fracture toughness test

3.6.1 Standard Test Method for Plane-strain Fracture Toughness of Metallic Materials E399

The standard E 399 is followed to perform the fracture toughness tests. In the corresponding subsection 2.6.3, the definition of plane strain condition is required for this test condition. This signifies that a crack tip resistance should be under a plain strain condition. The plane strain condition specifies that the thickness of the specimen must be large in comparison with the plastic deformed zone. In addition, the standard is valid for specimens with a thickness of 1.6 [mm] as minimum.

The standard ASTM E399 indicates that the specimens must be pre-cracked following the annex A2 [15] for bend specimens. The K_{Ic} value characterizes the material resistance to fracture

in an neutral environment of a specimens that contains a sharp crack subject to an intense external tension load. The K_{Ic} value can be applied for the designing of the components. The user must be aware of the difference between the service conditions and the test ones, since a component expose to aggressive environments will be fractured at a lower stress than the K_{Ic} value obtained at inert environment conditions [15].

The method presented can be utilized for purposes such as: research, developement and improvement of new or existing materials for their service function. It is also possible to evaluate the manufacturing impact, such as welding and metallurgic variables, like composition or heat treatments. All of these within the aim of selecting the suitable material for the component service conditions [15].

3.6.2 Fracture toughness test features

For this test there are 3 specimens per composition, the specimens are numbered N°1, N°2 and N°3. The compositions are the same as the ones in the table 3.1 and two round of tests will be performed.

3.6.3 Fracture toughness data acquisition equipment

For performing the pre-crack and the fracture toughness tests the Alwetron TCT 50 machine will be used, which works with an electromechanical system, see figure 3.5. The software named CycliEdc connected to the Alwetron machine allows to create methods for K_{Ic} determination and for cyclic loads, this latter mode is used to perform the pre-crack.

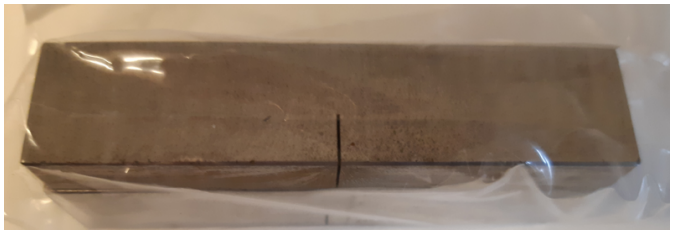

Figure 3.4: Bend specimen for the fracture toughness tests.

It can be seen in the figure 3.4, the notch is too narrow and it does not include the sharp edges to clip-on extensometer. The crack length for the pre-crack process is measured by using a portable microscope camera. For the fracture toughness test, it is mandatory to use an extensometer, no matter the type of specimen configuration. Consequently, the DIC (Digital image correlation) system will be used to record the test and the software TEMA to analyse the data. The DIC system offers a virtual extensometer tool, in which two points are selected and tracked during the test recording. The DIC allows to get a full strain field of the component. The data obtained

by the extensometer can be plotted versus the time, from where this chart, the timetable data is used and processed in MATLAB® . Must be remarked that using a simple unit conversion from a known dimension of the specimen- in this case the width (W)- and the equivalence in pixels will be applied to obtain the displacement in millimeters [mm].

To get the K_{Ic} value is needed to plot the force vs the displacement (due to the opening of the crack). The force data is acquired from the CycliEdc software, while the displacement, from the TEMA virtual extensometer. To merge both data (force and displacement) the software MATLAB® will be used.

Figure 3.5: Alwetron machine utilized for performing the pre-crack and fatigue toughness test.

3.6.4 Pre-crack method

The pre-crack procedure will be performed following the specifications in the annex A2 [15], some of these conditions are the ones below.

1. The pre-crack must be performed under cyclic loading for a number of cycles within the range of 10^4 and 10^6 m/cycle. The amount of cycles for the pre-crack depends on the specimens

dimensions (notch, width and thickness) and stress intensity level at which this process is performed.

2. The crack length, considering the started notch plus the pre-crack, must be in the range of 0.45 times the width (W) and 0.55 times the width.

3. The ratio of maximum stress intensity of the fatigue cycle over the young's modulus of the material$\left(\frac{K_{max}}{E}\right)$ shall not exceed 0.00032 [$\sqrt{m}$].

4. It is recommended that the load chosen for the initial part does not exceed 80 % of the K_{Ic} estimated. The stress intensity in the terminal stage, when 97.5% of the final crack length is reached, should not exceed 60 % of the K_{Ic}.

5. The frequency advisable should be under 100[Hz].

All these numbering were taking carefully in account since a wrong pre-crack can produce a severe impact on the K_{Ic} results, due to the high stress the material could experiment.

The K_{Ic} estimated value that is indicated in the item number 4 will be the maximum stress intensity observed from the fatigue crack growth test. To calculate the load to apply for reaching the 80 % of the estimated K_{Ic}, the expression in the annex for the bend specimen configuration will be used [15]. The corresponding expression can be seen in the equation below 3.8.

$$P = \frac{K \cdot B \cdot W^{1.5}}{f\left(\frac{a}{W}\right) \cdot S} \tag{3.8}$$

$$f\left(\frac{a}{W}\right) = f(d) = \frac{3 \cdot d^{0.5} \cdot (1.99 - d \cdot (1-d) \cdot (2.15 - 3.93 \cdot d + 2.7 \cdot d^2))}{2 \cdot (1 + 2 \cdot d) \cdot (1-d)^{1.5}} \tag{3.9}$$

Where:

P: load[KN].

K: estimated stress intensity [MPa $\sqrt{m}$].

B: specimen thickness in [cm].

W: specimen width in [cm].

a: specimen crack length in [cm].

s: span between the supports in [cm].

The units for this calculation have a great impact. Therefore, if the international system is used, the units should be the ones indicated above.

3.6.5 Fracture toughness calculation data interpretation

The procedure to follow, in order to calculate the fracture toughness, is the one in the standard ASTM E399 [15], specifically in the annex A3 [15] for bend specimens. Once the force and dis-

placement data are plotted, the next step is to calculate the conditional fracture toughness K_Q. To get this, first a secant line (yellow line in figure 3.6) must be drawn with a 0.95 % of the slope of the tangent line (red line in figure 3.6) to the linear part of the force vs displacement curve. The conditional load (P_Q)- is used afterward to calculate the conditional fracture toughness K_Q. The P_Q can be defined in two types depending on the curve demeanour, see figure 3.7. If the points that precede the intersection of the yellow line with the curve are lower than the load at the intersection itself, then P_Q is defined as the load at this intersection point (case for the curve 1 and 3 in the figure 3.7). The other situation is when there is a higher load value within the points previous to the intersection. In this case, as it is shown in the second curve in the figure 3.7, the P_Q is the maximum load of the points previous to the intersection.

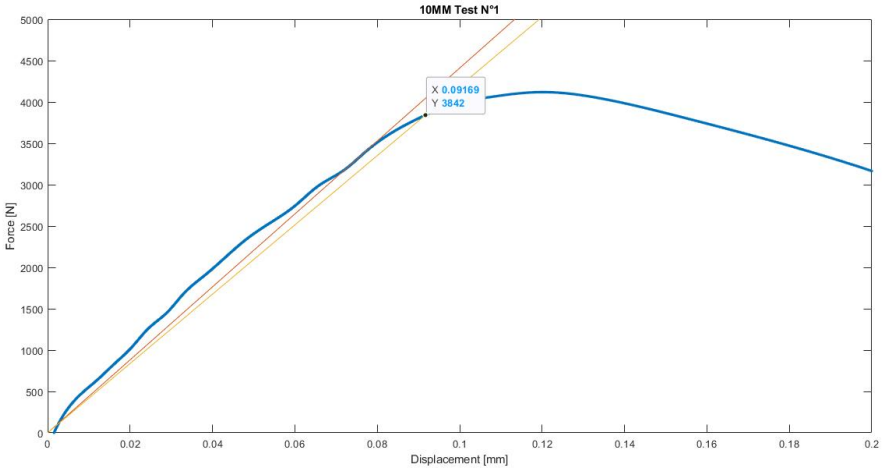

Figure 3.6: Chart of load [N] vs displacement [mm] for the specimen 10MM Pearlitic 0.5% nickel.

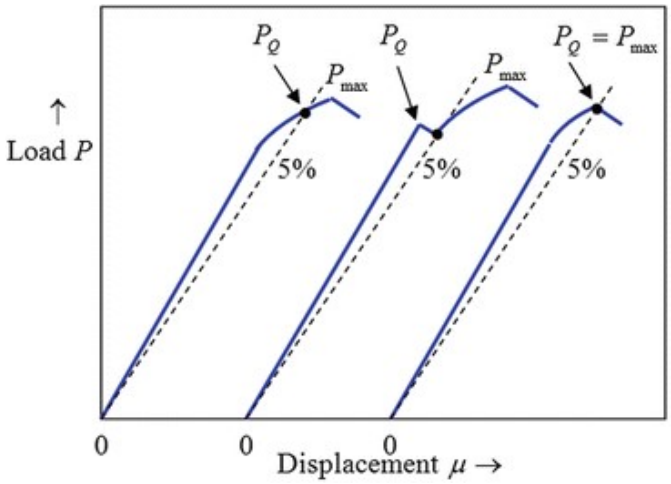

Figure 3.7: Types of load vs displacement curves.

Subsequently, the ratio $\left(\frac{P_{max}}{P_Q}\right)$ must be calculated, where P_{max} corresponds to the maximum load that the specimen can endure. If the value is under 1.10 the following step is to calculate K_Q as indicated in the annex A3 (see equation 3.10). Otherwise, the result is invalid, meaning that P_Q might not have any relation with K_{Ic}. The values used for the yield strength were the ones from the table 2 in the research, *"The Importance of the Microstructure for the Mechanical Properties of Compact Graphite Iron"* [39].

$$K_Q = \frac{P_Q \cdot S\cdot}{B \cdot W^{1.5}} \cdot f\left(\frac{a}{W}\right) \tag{3.10}$$

The terms in the equation 3.10 are the same ones as in the expression used for the pre-crack 3.8. Finally, the interpretation of the data, including all the steps described above, will be done creating a MATLAB® code.

Chapter 4

Results and Discussion

4.1 Fatigue crack growth rate results

4.1.1 Fatigue Crack Growth Rate as a function of the Stress Intensity Factor Range

For this section, it is relevant to establish the limits for the second stage of the crack growth rate versus the stress intensity factor range curves. In this stage, the fatigue crack growth rate has a linear demeanour, which can be described by the Paris' law expression, and it is mainly controlled by the stress intensity factor. According to the curves demeanor, it would be appropriate to settle this stage from 15 to 18 MPa$\sqrt{m}$.

A fatigue crack growth rate value, at a certain stress intensity factor range (within the second stage of the crack growth), is selected to make comparisons amongst the different samples curves. A reasonable value could be in the middle between the start of the curve and the final value obtained (the fracture toughness values). Therefore, the difference between an average of the fracture toughness values and the starting value of 14 MPa$\sqrt{m}$ could be suitable to be utilized. Although, from the procedure mentioned, the value would be 15.5 MPa$\sqrt{m}$, which is quite closer to the initiation of the second stage. Hence, using 17 MPa$\sqrt{m}$ of stress intensity factor range as the comparison value assures that the specimens are in the linear region. Consequently, the Paris' law expression can be used to calculate the fatigue crack growth rate.

- **Ferritic and pearlitic specimens**

  There are no substantial differences between the curves in the figure4.1. Nonetheless, a tendency can be observed where, for the same value of stress intensity factor range, the pearlitic specimens display lower fatigue crack growth rate compared to the ferritic specimens. This demeanor shows that a crack, in a specimen with a pearlitic matrix undergoes a slower

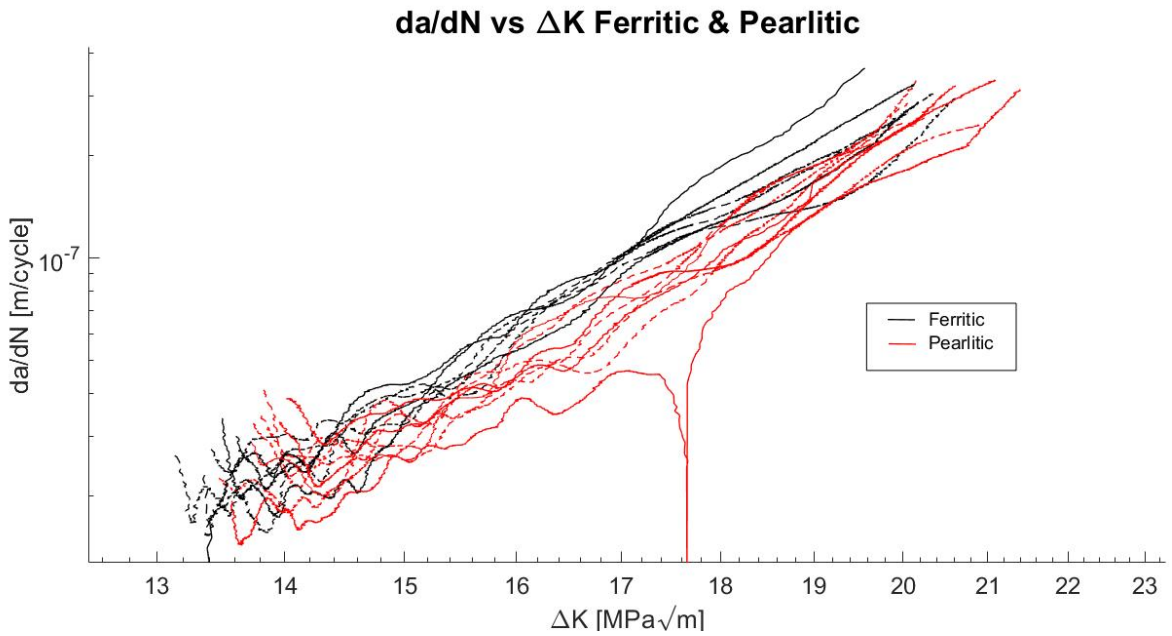

Figure 4.1: Fatigue crack growth rate versus the stress intensity factor range for the pearlitic and ferritic specimens, tests N°1 and N°2.

propagation than a ferritic specimen. A slower fatigue crack growth rate is a beneficial property for a cylinder's head material, meaning a higher fatigue strength.

At the initial part of the curve, there is a high level of noise in the data, which does not allow the possibility of appreciating a clear first stage of the curve or even identifying the fatigue crack growth threshold. See figure 2.7. The noise, and especially the drop in the data around 17.6-17.8 MPa$\sqrt{m}$, can be caused when the extensometer is not in the right position at that precise time of the test.

- **Ferritic specimens**

  For the ferritic specimens, the influence of molybdenum (0.25% and 0.15 %) was analyzed and compared with a reference composition (0,05% Mo)[1]. In the figure 4.2, there is no clear trend independently of the molybdenum amount. This shows that molybdenum seems to have no impact on the fatigue crack growth rate for alloys with a ferritic matrix. The variation of the fatigue crack growth rate for the ferritic specimens at 17 MPa$\sqrt{m}$ is of $9.58{\cdot}10^{-8}$ (0.15% Mo) to $1.04{\cdot}10^{-7}$ $\frac{m}{cycles}$ (0.25% Mo) 6.2.

[1]RC: is the anachronism for "reference composition" that will be used as denotation.

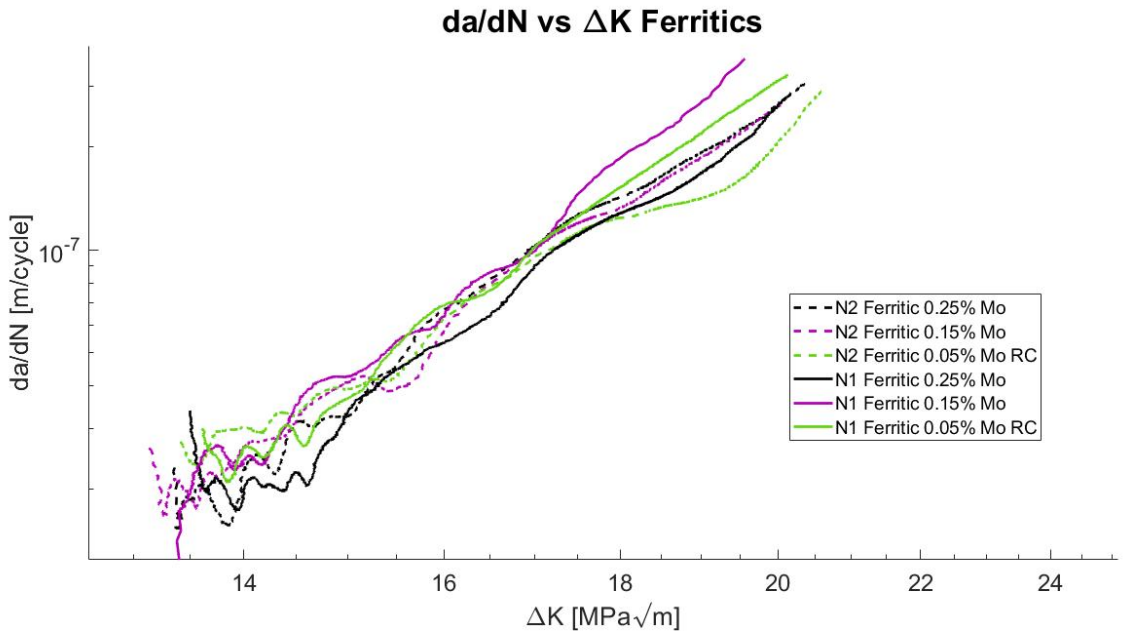

Figure 4.2: Fatigue crack growth rate versus the stress intensity factor range for the ferritic specimens, tests N°1 and N°2 included.

- **Pearlitic specimens with molybdenum**

  The effect of molybdenum on the fatigue crack growth rate was studied for the pearlitic specimens as well. For this case, an evident tendency yet not large was noted. In the figure 4.3, the specimens that contain molybdenum in their chemical composition (green curves) tend to allocate under the reference composition curves (red) throughout the test, especially in the range of 15.5-18 MPa$\sqrt{m}$. This means that the molybdenum aids to decrease the fatigue crack growth rate. The demeanor mentioned sustains the effect of molybdenum as a graphite refiner, which can also have an impact on the pearlitic matrix, since it can reduce the inter layers space of the ferrite and cementite incrementing the strength of the material. The variation of the fatigue crack growth rate at 17 MPa$\sqrt{m}$ for the pearlitic specimens go from $8.18{\cdot}10^{-8}$ (pearlitic RC) to $4.86{\cdot}10^{-8}$ $\frac{m}{cycles}$ (0.25 % Mo) 6.2.

  For the final stage of the curves, the molybdenum does not show a great impact on the fatigue crack growth rate. Therefore, no conclusions about the effect of Mo on this region can be made. In addition, it must be considered that at the last stage, the crack growth will depend strongly on the microstructure, the mean stress, and the thickness of the component.

  In summary, according to the results obtained, there is a tendency for pearlitic specimens to display lower fatigue crack growth rate values as the molybdenum shows a positive impact on this property. On the contrary, the molybdenum has no relevant effect on the ferritic specimens.

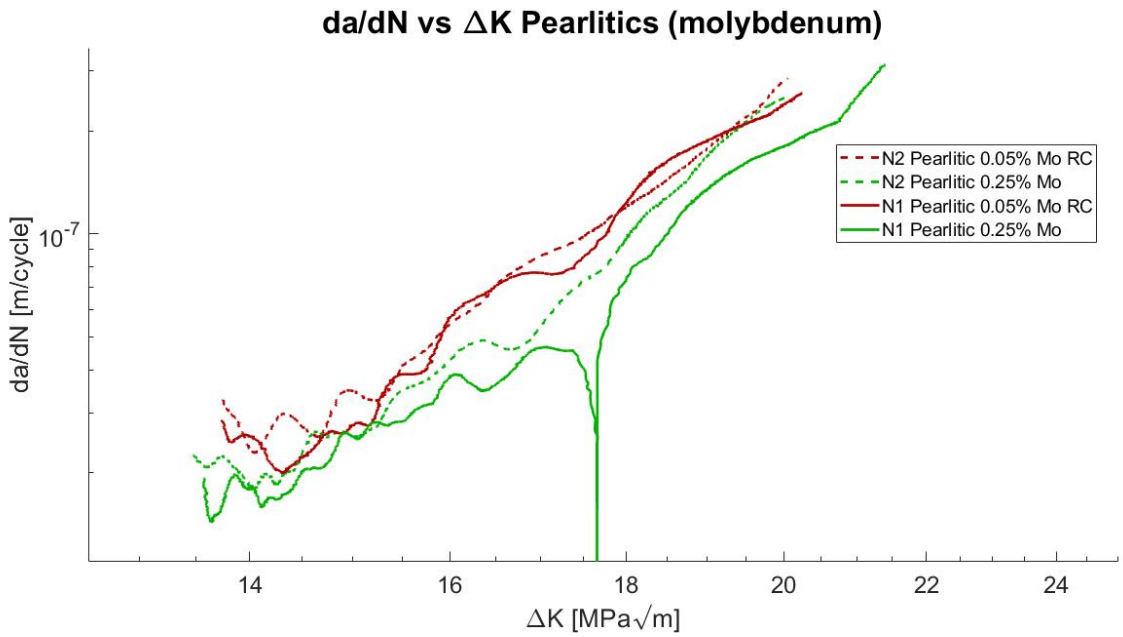

Figure 4.3: Fatigue crack growth rate versus the stress intensity factor range for the pearlitic specimens with molybdenum and reference composition, including tests N°1 and N°2.

- **Specimens with nickel**

  The effect of nickel on the fatigue crack growth rate property was at most analized for pearlitic specimens. In the figure 4.4, there is no clear effect of the nickel on the fatigue crack growth rate curves noted until 17.8 MPa$\sqrt{m}$. From this value of the stress intensity factor range, the specimens with a larger amount of nickel (1%) tend to locate beneath the rest of the curves. No apparent effect was shown for the specimens with 0.5 % Ni, these curves are quite similar to those of the reference composition.

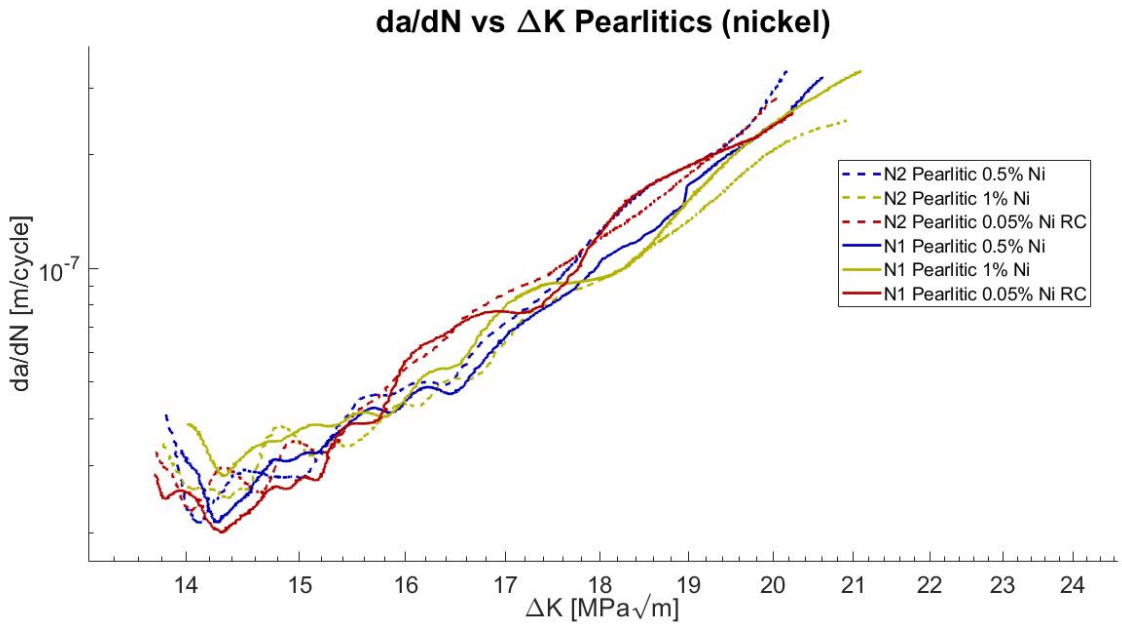

Figure 4.4: Fatigue crack growth rate versus the stress intensity factor range for specimens with nickel and reference composition. Tests N°1 and N°2 included.

From the results, it can be stated that the adequate amount of nickel (from 1%) has a positive impact since the crack propagation becomes slower for the pearlitic specimens from 18 MPa$\sqrt{m}$. This can be related to the soft refiner effect of the nickel on the pearlite layers, see section 2.8.

- **Pearlitic specimens**

  The figure 4.5 contains all pearlitic specimens, and it allows to analyze the effect of the molybdenum and nickel in comparison with the reference composition. For the section of the stress intensity factor range of 15-18 MPa$\sqrt{m}$ it is possible to observe that the curves with 0.25% Mo are situated beneath the rest of the other ones. From 18 MPa$\sqrt{m}$ until the end of the test, the reference composition curves tend to stay onto, displaying faster fatigue crack growth rate curve conduct, while the ones corresponding to 0.25% Mo and 1% Ni stay below.

  Both conducts described can be understood via the effect of the alloying elements, Mo and Ni. The graphite refinement effect of the molybdenum is greater for pearlitic specimens since it is not only about the impact on the graphite but on the pearlite layers as well. More refined graphite and thinner pearlite layers increase the strength of the alloy. This effect was best appreciated for the specimens with 0.25 % Mo. And as for the nickel, it contains a graphitizing effect. Thus, it is expected to observe a clearer impact on the hardness of the alloy than on the fatigue crack growth rate. Further, it is been noted that the nickel produces

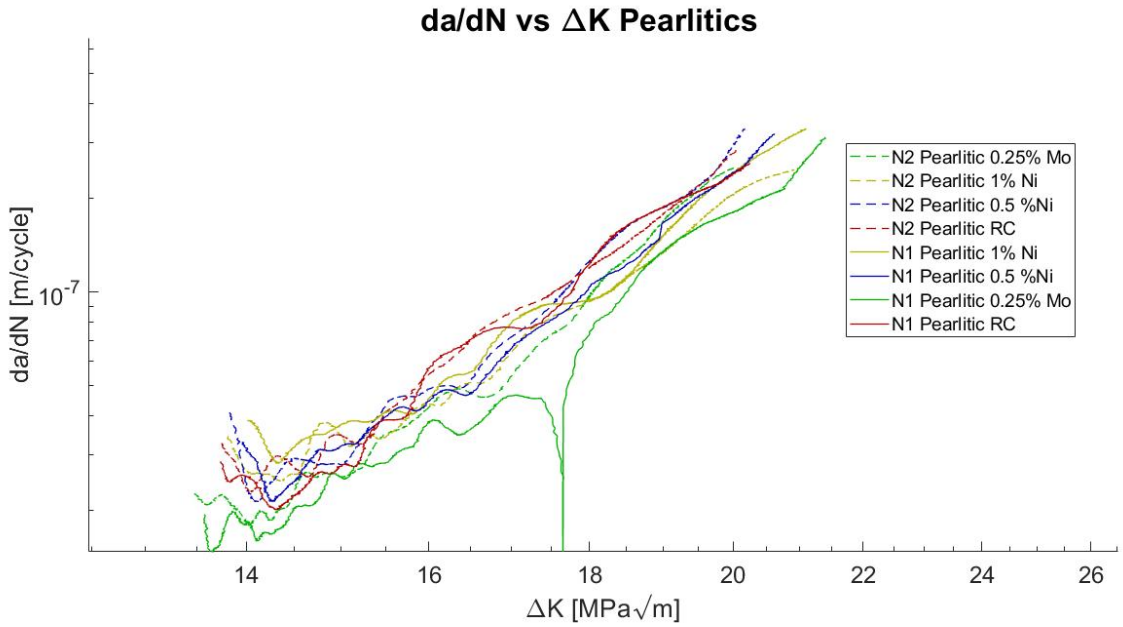

Figure 4.5: Fatigue crack growth rate versus the stress intensity factor range for pearlitic specimens. Includes tests N°1 and N°2.

a soft graphite refinement effect. This effect along with the graphitizing one, contributes to having slower fatigue crack growth rate for the specimens containing 1% Ni. Although, the fatigue crack growth rate values at 17 MPa$\sqrt{m}$ 6.2 do not show major differences. There is an impact of the alloying elements where the ones with the lower values were the specimens with 0.25% Mo and 1% Ni, $4.86{\cdot}10^{-8}$ $\frac{m}{cycles}$ and $6.97{\cdot}10^{-8}$ respectively.

4.1.2 Relation between fatigue crack growth rate and graphite aspect ratio

The graphite aspect ratio is defined as the length (a) over the width (c), $\frac{a}{c}$. For a graphic view, see the figure 2.3 in the literature review chapter 2. According to this information, a big value of aspect ratio represents a graphite morphology comparable to a flake (vermicular). On the contrary, a small value means that the graphite appears to be closer to nodules.

To get a reliable conclusion from the graphite aspect ratio values, it is important to set the limits to define whether the graphite resembles a flake either compact or closer to nodular morphology. Considering the values obtained of aspect ratio and its standard deviation for different alloys in the research "On the correlation between microstructural parameters and the thermo-mechanical fatigue performance of cast iron" [11], the lamellar graphite iron studied LGI290 had an aspect ratio of 13.88, while the compacted cast irons (CGI400 ferritic, CGI350 ferritic/pearlitic and CGI400 pearlitic) were between 4.12 to 4.94 depending on their chemical composition and matrix, and the

spheroidal graphite iron specimen (SiMo51) had an aspect ratio of 1.85, see table 4.1.

Denotation	Matrix	Aspect ratio [-]
LGI290	pearlitic	13.88 ± 0.85
CGI400	ferritic	4.83 ± 0.32
CGI350	ferritic/pearlitic	4.12 ± 0.13
CGI400	pearlitic	4.94 ± 0.29
SiMo51	ferritic	1.85 ± 0.16

Table 4.1: Denotation, type of matrix and graphite aspect ratio values for the specimens tested in the research "On the correlation between microstructural parameters and the thermo-mechanical fatigue performance of cast iron" [11].

A more graphic representation of the difference in the aspect ratio values for different types of irons can be observed in the figure 4.6.

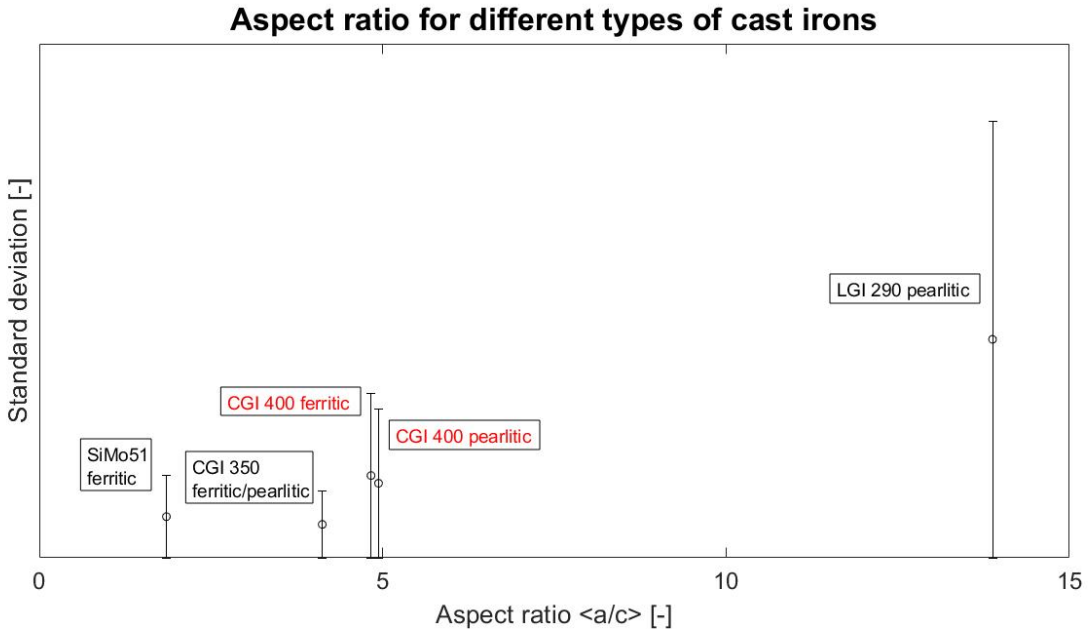

Figure 4.6: Chart of aspect ratio for lamellar (LGI290), compacted (CGI400, CGI350) and nodular iron (SiMo51) tested in the research paper "On the correlation between microstructural parameters and the thermo-mechanical fatigue performance of cast iron" [11].

The research document named "The casting procedure's impact on the microstructure" [38], measured the graphite aspect ratio values and the corresponding standard deviation for the same specimens compositions as in this research, see table 4.2.

In consideration of the aspect ratio values, see table 4.2, it is possible to see that the magnitude is within the range for the compacted graphite irons shown in the table 4.1. Therefore, it is feasible to discard the fact of analyzing specimens either fully flake or nodular graphite morphology.

Matrix	Composition			Aspect Ratio [−]
	%Mo	%Ni	%Si	
Perlitic	0.05	0.05	2.30	5.07 ± 0.012
	0.25	0.05		4.02 ± 0.261
	0.05	0.50		5.08 ± 0.090
	0.05	1.00		4.77 ± 0.036
Ferritic	0.05	0.05	4.00	4.49 ± 0.056
	0.15	0.05		4.54 ± 0.066
	0.25	0.05		4.43 ± 0.039

Table 4.2: Graphite aspect ratio values, chemical composition and type of matrix for the specimens analysed in this document.

The silicon is a relevant element for the cast iron chemical composition due to its graphitizing effect. It is added in quantities of 1%-3%. In the table 4.2 can be observed that the pearlitic specimens have 2.3% of Si, while the ferritic samples have 4% instead. The amount of silicon and carbon contributes to the type of matrix the cast iron displays at a settle cooling rate. According to the literature (see [42]) at a normal cooling rate with 3.22% of C and 4% of Si the matrix that will be developed is a ferritic one, while for 3.65% of C and 2.3% of Si will be pearlitic. Therefore, the silicon composition of samples only impacts on the type of matrix obtained. Consequently, this difference of the silicon compositions does not have a direct effect on the properties to analyze, such as fatigue crack growth rate, fracture toughness, graphite aspect ratio and hardness.

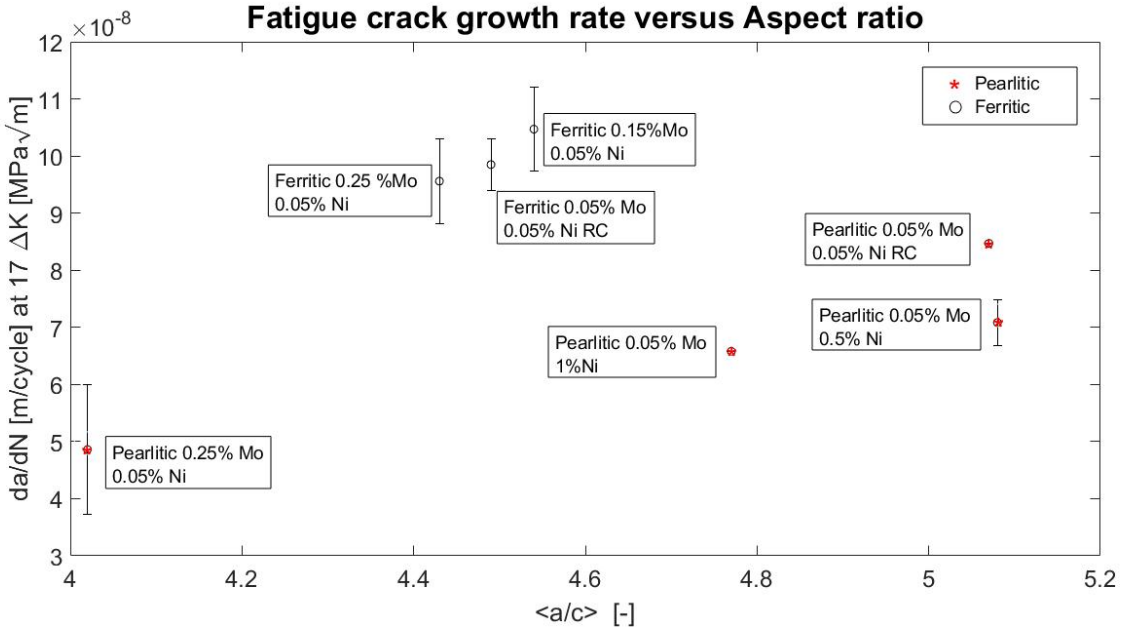

Figure 4.7: Fatigue crack growth rate at 17 MPa$\sqrt{m}$ versus aspect ratio for all specimen tested.

It is possible to identify some trends amongst the fatigue crack growth rate, aspect ratio, and

alloying elements. The pearlitic specimens with %0.5 Ni and pearlitic RC had the higher aspect ratio values. This means that there are higher probabilities of finding lamellar graphite compared to the rest of the specimens 4.7. Within the pearlitic group samples, the alloy with 1% Ni has a considerably smaller aspect ratio in comparison to the samples with 0.5% Ni and reference composition, this might occur due to the soft graphite refinement effect.

The smaller values of graphite aspect ratio observed were for the specimens that contain 0.25% molybdenum, 4.02 and 4.43 for the pearlitic and ferritic respectively. This confirms the great impact that molybdenum has on the graphite morphology. It can also be observed, that for the ferritic specimens there is no positive effect of the alloying elements on the fatigue crack growth rate. Thus, the higher rate value corresponds to the ferritic specimen with 0.15% Mo 6.2.

From the results obtained, it can be stated that the type of matrix appears to have a more significant impact on the fatigue crack growth rate than the alloying elements. Moreover, the addition of molybdenum tends to decrease the graphite aspect ratio. The combination of a pearlite matrix with molybdenum displays better fatigue crack growth rate performance. This can be related to the fact that graphite acts as pre-existing cracks. Thus, the lower the aspect ratio is, the higher the probabilities of finding more nodular graphite will be, which means that it concentrates less stress, reducing the pre-crack effect of it. The type of matrix affects the crack growth as well, whereas in a pearlitic matrix the crack needs to propagate through layers of cementite and ferrite, which can be crossed, making the crack propagation more complicated than it might be for a ferritic matrix.

4.1.3 Relation between fatigue crack growth rate and hardness

The research document named "The Importance of the Microstructure for the Mechanical Properties of Compact Graphite Iron" [39], measured the hardness and the corresponding standard deviation for the current research alloys, see table 6.3.

A clear trend is identified between the type of matrix and the hardness. In figure 4.8, the pearlitic specimens display lower fatigue crack growth rate, which also contains higher hardness values.

The ferrite is a phase that contains a low carbon solubility (0.008%C). Consequently, few carbon atoms deform the crystal lattice by staying in the middle of the edge or in the center of faces of the cell unit [43]. Therefore, there is a low mobility resistance for the dislocations, which gives the ferrite a ductile phase characteristic with lower hardness.

Meanwhile, a pearlite matrix is composed of two different phase layers, ferrite, and cementite (6.67%C), in the proportion of 86.5% and 13.5% correspondingly. Cementite is a hard and brittle phase due to the high containing carbon amount. Taking this information into account, a pearlite matrix displays a higher hardness, which can be due to the percentage of cementite.

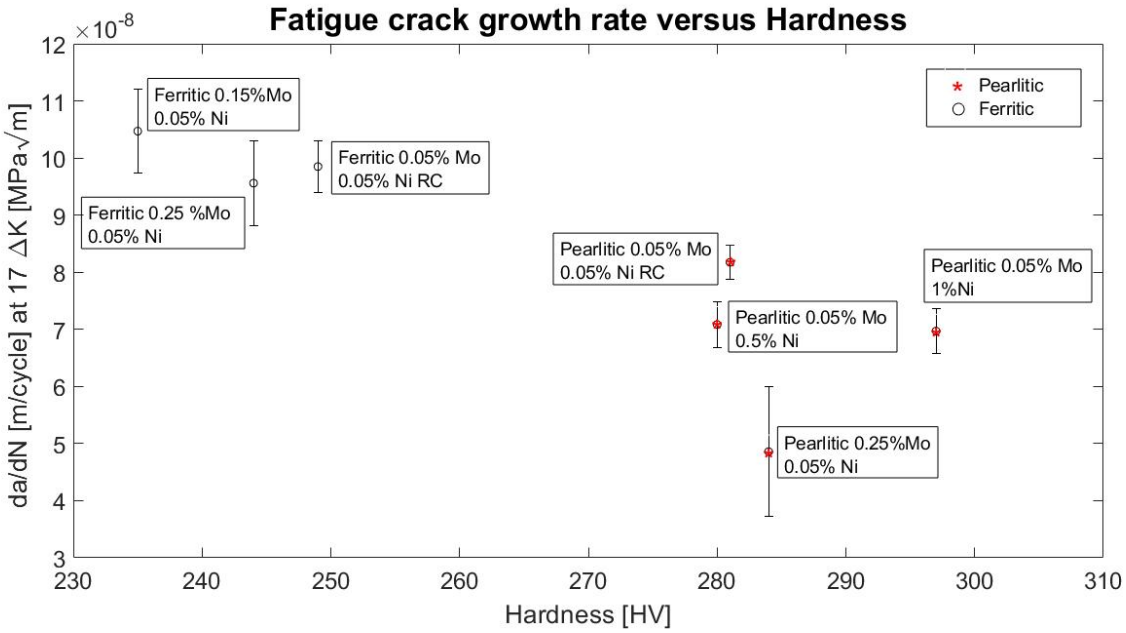

Figure 4.8: Fatigue crack growth rate at 17 MPa$\sqrt{m}$ versus hardness of all specimen tested.

In the same figure (4.8), it is possible to observe that the molybdenum has little influence on the hardness of the material for the ferritic specimens. Furthermore, it appears to decrease it. This can be due to the molybdenum graphite refinement effect. And since the graphite is inserted in a matrix roughly receiving carbon, the chance for the molybdenum to express its effect is minimal. On the contrary, for the pearlitic specimens, the alloying elements seem to have an impact on the hardness and fatigue crack growth rate, which was proven and clarified in the previous subsections (see, 4.1.1 and 4.1.2). It must be considered that the molybdenum can lessen the space between the layers of the pearlite, increasing the hardness of the alloy. It is expected that the higher the amount of nickel, the greater the hardness. Since it is a graphitizing element, and graphite is a hard and brittle phase. A 0.5% Ni is not sufficient to observe the effect of the nickel. Nevertheless, a 1% produces an impact on the alloy. Consequently, it is the one with the higher hardness of the specimens tested.

4.1.4 Analysis of the Paris' law constants, C and m, with the values reported

The table 4.3 shows an average of the constants C and m for the specimens N°1 and N°2 tested. The values were obtained through a linear approximation of the fatigue crack growth rate versus stress intensity factor range curves from the range of 15 to 18 [MPa$\sqrt{m}$]. To obtain a linear relation between the fatigue crack growth rate versus the stress intensity factor range chart, the curves must be plotted in a logarithmic scale. Therefore, the logarithm of C is the intercept and

Matrix	Composition			C	m
	%Mo	%Ni	%Si		
Perlitic	0.05	0.05	2.30	$1.87 \cdot 10^{-17}$	7.84
	0.25	0.05		$3.57 \cdot 10^{-10}$	3.88
	0.05	0.50		$1.77 \cdot 10^{-15}$	6.44
	0.05	1.00		$1.86 \cdot 10^{-15}$	6.15
Ferritic	0.05	0.05	4.00	$6.44 \cdot 10^{-17}$	7.48
	0.15	0.05		$1.79 \cdot 10^{-17}$	7.98
	0.25	0.05		$4.10 \cdot 10^{-17}$	7.91

Table 4.3: Paris' law constants C and m from the fatigue crack growth rate versus stress intensity factor range curve for all the specimens tested.

m corresponds to the slope of the lineal part of the curve. All things considered, the C and m constants give information related to the demeanor of the curve.

If C is high (in comparison with the values of other curves), the curve will be located above the plot. In addition, the bigger m is, the steeper the curve will be. Consequently, if m is high and C low, the curve will be located in the inferior part of the chart and will have a steep conduct. The combination of curves located in the lower part of the chart with a moderate or small m value shows a better response to the fatigue crack growth. Therefore, a slower rate for the crack propagation. Although, if m is high the crack will grow at a high rate.

From the values reported in the table 4.3, can be seen that the constants do not significantly differ, except for the pearlitic specimen with 0.25% Mo. Which, the C constant has between 5 to 7 magnitude difference orders and around 4 units of difference for the m constant. The alikeness within the Paris' law constants for the rest of the specimens is not unusual since they are the same type of irons (compacted cast irons). They, all in all, differ in the matrix and the amount of alloying elements. Withal, an inconsistency was found between the values reported in the paper and those obtained in this research. For the values informed, the lower m values were for the ferritic specimens, while in the current research were for the pearlitic samples.

The pearlitic specimens, except for the reference composition sample, tend to have lower values of the m constant. The pearlitic specimen with 0.25% Mo is the one with the lowest m, in other words, a less steep slope. This constitutes that the curve displays a progressive crack growth. The second specimen with a low value of m is the pearlitic 1% Ni, followed by the pearlitic with 0.5% Ni. From these results, it can be evinced that the alloying elements have a favorable influence on the pearlitic specimens, as was stated in the fatigue crack growth rate tests analysis. Contrastingly, for the ferritic specimens the alloying elements are not a precedence for the specimen fatigue crack growth demeanor, which was also observed in the previous analysis of the curves.

The specimens with the more substantial values of C correspond to the pearlitic with 0.25%

Mo and to the one with 1% Ni. Even though the C value is relevant, since it is the intercept of the curve, it was noted that does not impact the curve demeanor on the same scale as the m constant value.

All things considered, there is a congruence for all the results of the fatigue crack growth rate tests. The pearlitic specimens tend to display better performance. In addition, the alloying element, such as molybdenum and nickel, appears to improve the specimen response to this test, especially those with a composition of 0.25% Mo. On the other hand, the ferritic specimens tend to have higher crack propagation and no relevant influence from the alloying elements.

Concerning the values informed in the table 2.1, there is a bigger difference between the m and C Paris' law values obtained. This is related to the fact that several degrees of vermicularity were analyzed. It is possible to identify that specimens with higher C and m constants values are those that have a flake graphite morphology or a high vermicularity (90 %). Therefore, the curve of the specimens that have flake graphite tends to be positioned above the rest of the curves showing a fast progression of the crack growth (steep curve). The m constant values attained for the specimen tested in this research were similar to the ones obtained for a 10 % and 50 % of vermicularity informed. The order of magnitude of the C constant was also between this range of vermicularity. Therefore, the values of the Paris' law constants obtained in this research coincided with a lower vermicularity than expected, since they were closer to the samples with 10 % informed.

In accordance with the results in the "Fracture toughness and crack growth rate for ferritic and pearlitic compacted cast irons at 25 °C and 150°C" paper (see table 2.1), the ferritic specimens displayed lower values of m and C than those pearlitic ones for the same vermicularity degree. On the contrary, this trend contrasted with the specimens tested in the current research. The pearlitic specimens showed better fatigue crack growth rate performance, in which smaller values of m and C were achieved compared to the ones for the ferritic specimens.

Comparing the values in both tables, (2.1 and 4.3), the average values of C and m for the specimens tested in this research were similar to those for a vermicularity of 50 %. Specifically for the pearlitic specimens with 0.25% Mo and 1% Ni, they are closer to the values for the samples with a low vermicularity (closer to nodular graphite), this confirms the effect that alloying elements have on the fatigue crack growth rate conduct.

4.1.5 Validation of the crack length measures

During all the fatigue crack growth rate tests, the crack length was measured using several methods. The initial measures were made with a vernier caliper and the Doli software. The last-mentioned was measured by an extensometer attached to the sharp edges of the C(T) specimens. Once the test was ongoing, the crack length was continuously measured with the software. The DIC system was used to measuring the crack lengths at certain moments during the test (without disassembling

the specimen). The final crack length records were obtained with the software Doli and the Leica optical microscope.

The validation of the crack length was realized for both the initial and final measure. The ones taken in the middle of the tests are not comparable , since their timing within the test was different while being measured. It is key to validate the crack length values, especially for the final measure since by the end of the fatigue crack growth test, the propagation of crack was uncontrolled, and it made the extensometer come out. Therefore, it is probable that the last software crack length record is not accurate. The expression 4.1 shows the calculation procedure for validating the measures.

$$\frac{\mid software\, measure - physical\, measure \mid \cdot 100}{physical\, measure} \tag{4.1}$$

Where:

software measure : crack length value from the Doli software.

physical measure : crack length value measured with a vernier caliper (initial measure) or from the Leica microscope software (final measure).

The table 4.4 shows the crack length values measured and the corresponding error for all the first round of specimens. It is probable to observe a large error for the final crack length, except for the 26MM (ferritic 0.15% Mo) specimen. This result was expected due to the situation with the extensometer by the end of the test. Although, in this research, the final measure does not influence considerably the fatigue crack growth rate versus stress intensity factor range curves, since the extensometer failure was in the moment in which the specimen increased the crack length from 16 [mm] to 21[mm] in less than a second.

Specimen	Condition	Software measure [mm]	Physical measure [mm]	Error
1MM	Initial	10.04	9.77	2.76
	Final	15.98	21.07	24.15
4MM	Initial	9.81	9.94	1.30
	Final	15.86	21.00	24.48
10MM	Initial	9.98	10.08	1.02
	Final	16.03	21.82	26.53
16MM	Initial	9.89	9.97	0.82
	Final	15.81	20.4	22.49
20MM	Initial	9.82	10.02	1.96
	Final	15.65	20.47	23.55
26MM	Initial	9.91	10.02	1.13
	Final	15.85	10	1.08
36MM	Initial	9.81	9.94	1.30
	Final	15.88	21	24.39

Table 4.4: Error for validation of the crack length considering the initial and final value obtained through the software and physical measures.

4.2 Fracture toughness results

4.2.1 Fracture toughness values

To obtain the fracture toughness values the methodology explained in the subsection 3.6.1 was followed. The values in the table 4.5 correspond to the average for both rounds of tests. The values of fracture toughness for the specimens tested do not differ in more than 11 units $[MPa\sqrt{m}]$. The influence of the alloying elements on the pearlitic specimens is easily identified, the highest value of fracture toughness was observed through the pearlitic specimens with 0.25% Mo (37.39 [MPa$\sqrt{m}$]). For the ferritic specimens containing molybdenum is not possible to confirm an effect of this element on the fracture toughness, since the values within this group are quite similar. The nickel appears to have a negative impact on the fracture toughness displaying the lower values from all the specimens tested, 25.82 and 25.62$[MPa\sqrt{m}]$ for 0.5% Ni and 1% Ni respectively. This demeanor is consequent with the graphitizing effect of the nickel, which increases the hardness, hence the alloys turn more brittle.

Matrix	Composition			$k_{Ic}[MPa\sqrt{m}]$	$P_Q[N]$
	%Mo	%Ni	%Si		
Perlitic	0.05	0.05	2.30	31.09	4884.20
	0.25	0.05		37.39	5870.25
	0.05	0.50		25.82	4130.00
	0.05	1.00		25.62	4104.95
Ferritic	0.05	0.05	4.00	29.31	4646.60
	0.15	0.05		28.68	4477.75
	0.25	0.05		29.63	4579.95

Table 4.5: Values of fracture toughness, k_{Ic}, and the corresponding load P_Q for the specimens analyzed.

The fracture toughness values for pearlitic and ferritic reference composition specimens (the ones with 0.05% Mo and 0.05% Ni in table 4.5) do not vary significantly. Therefore, the alloying elements seem to have a relevant influence on the fracture toughness in comparison with the type of matrix.

In consideration of the fatigue crack growth rate and fracture toughness results, it can be stated that the alloying elements do not seem to have a benefit for the ferritic specimens.

In the figure 4.9 there is a graphical representation of the tendencies previously explained. The specimens with nickel tend to be in the lower part of the figure since they displayed the lower fracture toughness values. It is likely to observe that the ferritic specimens show very similar values. Therefore, there was no improvement observed in the fracture toughness values of the ferritic specimens.

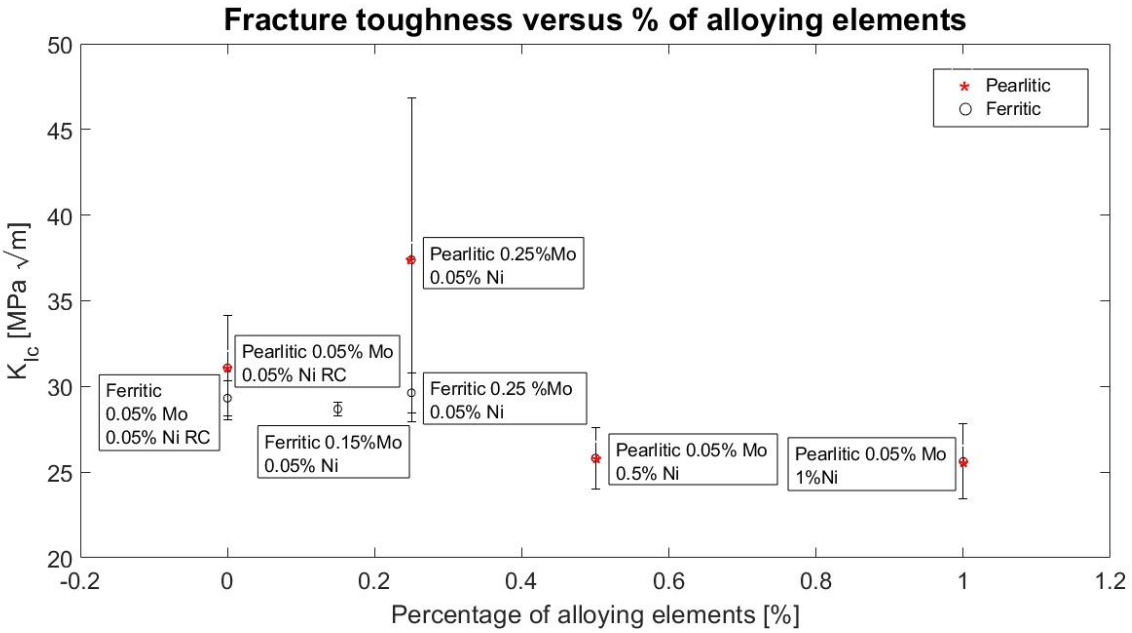

Figure 4.9: Relation between the fracture toughness values and the amount of alloying elements for the compositions tested.

Although, the molybdenum appears to have a positive impact on the pearlitic specimens increasing the fracture toughness value in 6.30 $[MPa\sqrt{m}]$ compared with the reference composition. There is a clear trend of the nickel influence on the fracture toughness for the pearlitic specimens. The higher the amount of nickel, the lower the fracture toughness value. This demeanor occurs due to the graphitizing effect, which raises the hardness of the alloy turning it more brittle. The difference between the highest value and the lowest (pearlitic with 0.25% Mo and pearlitic 1% Ni respectively) is significant with a value of 11.77 $[MPa\sqrt{m}]$.

All things considered of both test results, there is a tendency for the pearlitic specimen with 0.25% of molybdenum to show slower fatigue crack growth rate and higher fracture toughness than the rest of the samples analyzed. The effect of the molybdenum as a graphite refiner permits to concentrate less stress. Thereby, the combination of a matrix with higher strength, and the effect of molybdenum displays a better performance in the fatigue crack growth and fracture toughness tests.

The nickel appears to be an alloying element that, grants a higher hardness, but lower fracture toughness due to its graphitizing effects. The graphite corresponds to the hardest and most brittle phase within the samples' microstructure. However, a favorable effect of the nickel was identified on the fatigue crack growth rate and aspect ratio.

Comparing the fracture toughness values attained with the ones informed in the research paper "Fracture Toughness and Crack Growth Rate of ferritic and pearlitic Compacted graphite irons at 25°C and 150°C" [7], see table 2.1. It is likely to notice smaller values in this research compared to

the specimens with 90 % vermicularity reported (43 and 56[MPa$\sqrt{m}$] for the ferritic and pearlitic respectively). Although, the values of fracture toughness are bigger than for the lamellar graphite (22 and 14[MPa$\sqrt{m}$] for the ferritic and pearlitic respectively). It was expected for the specimens of this research to display similar values to the samples with 50 % vermicularity, considering the comparison between the C and m Paris' law constants. This considerable vast difference between the values informed and the ones attained from the tests could be influenced by several factors, such as data acquisition technology, test conditions, and parameters.

In the reported values, there is a better performance for the fracture toughness property with the pearlitic specimens. In the tests of this research, there was a greater influence of the alloying elements than the type of matrix, where the molybdenum appears to improve the fracture toughness of pearlitic specimens.

4.2.2 Relation between the fracture toughness and graphite aspect ratio

As it was previously explained, a higher graphite aspect ratio value indicates a similar to a flake graphite morphology, while a smaller value resembles a nodular or spheroidal graphite morphology. The specimens tested are within the expected range for compacted graphite. The pearlitic specimen with 0.25% Mo is the one that presents the lowest aspect ratio value, and the highest fracture toughness value, confirming the effect of molybdenum graphite morphology changes, which allows a better stress dissipation through the specimen microstructure.

In the figure 4.10, it is plausible to observe a significant influence of the alloying elements compared to the type of matrix on the fracture toughness, where the pearlitic specimen with 0.25% molybdenum shows the highest fracture toughness and the lowest aspect ratio value.

The ferritic specimens, which are the ones with a lower aspect ratio (after the pearlitic 0.25% Mo), do not display the second higher value of fracture toughness. They tend to have similar values to the pearlitic reference composition specimens. This confirms the least and almost nonexistent effect of the alloying elements on the ferritic matrix samples.

Moreover, it must be mentioned the clear and relevant influence of the molybdenum as a graphite refiner. The specimens with an amount of 0.25% Mo in their composition, either pearlitic or ferritic, have the smaller aspect ratio values. For the pearlitic specimens, the effect of the molybdenum improves the fatigue crack growth rate and fracture toughness as well, since the morphology of the graphite will concentrate less stress, allowing a higher resistance to the fracture toughness test.

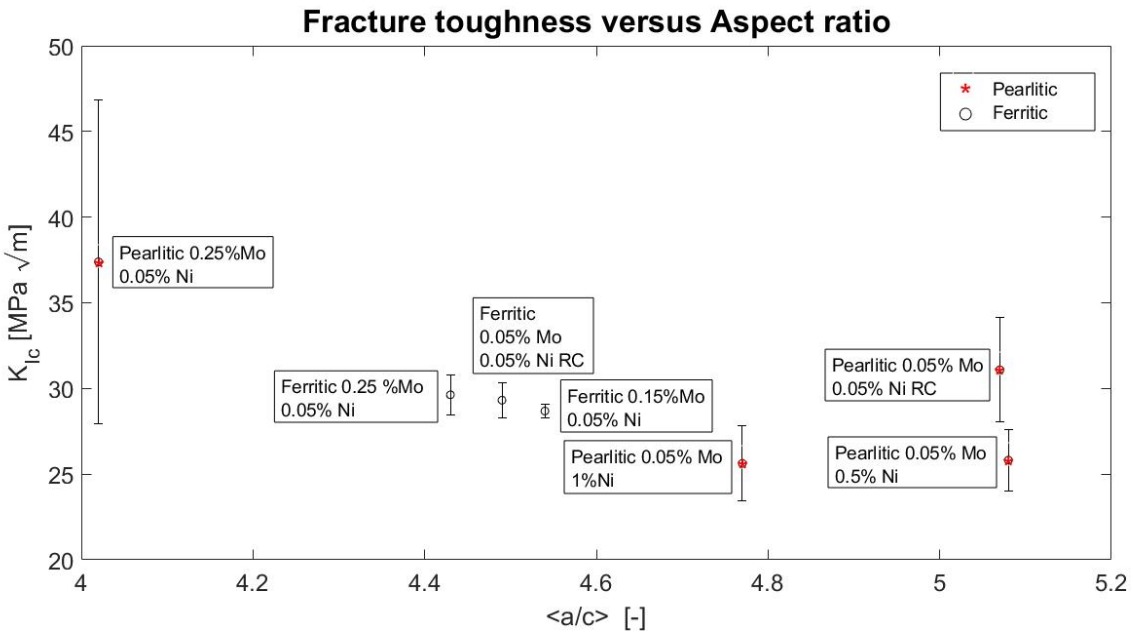

Figure 4.10: Relation between fracture toughness and graphite aspect ratio values for the specimens tested.

4.2.3 Relation between fracture toughness and hardness

The influence of the type of matrix on the hardness of the alloy is evident, see figure 4.11. The alloys with lower hardness are the ferritic ones since this matrix is more ductile than the pearlitic. Although the tendency is clear for the type of matrix on the hardness, it needs to be mentioned that the difference within the fracture toughness values is not substantial.

From this figure, it is likely to appreciate the graphite refinement effect of the molybdenum which produces a relevant increase in the fracture toughness resistance and hardness of the alloy.

For the pearlitic specimens, the alloy with 0.25% Mo presents the most advantageous combination of properties. Concerning the hardness, the alloy is the second with a higher value. Although, it is not the most brittle one, since it is the one with the highest fracture toughness of the specimens tested. Simultaneously, the pearlitic alloy with 0.25% Mo has the smallest graphite aspect ratio value and the slowest fatigue crack growth rate test at 17 MPa$\sqrt{m}$ 6.2, with the smallest m Paris' law constant value.

The nickel influence was only analyzed for the pearlitic specimens, which turns them more brittle, displaying an increase in the hardness of the alloy observed for the samples with 1% Ni. Therefore, this latter has the lowest fracture toughness, and the highest hardness values from all the compositions analyzed.

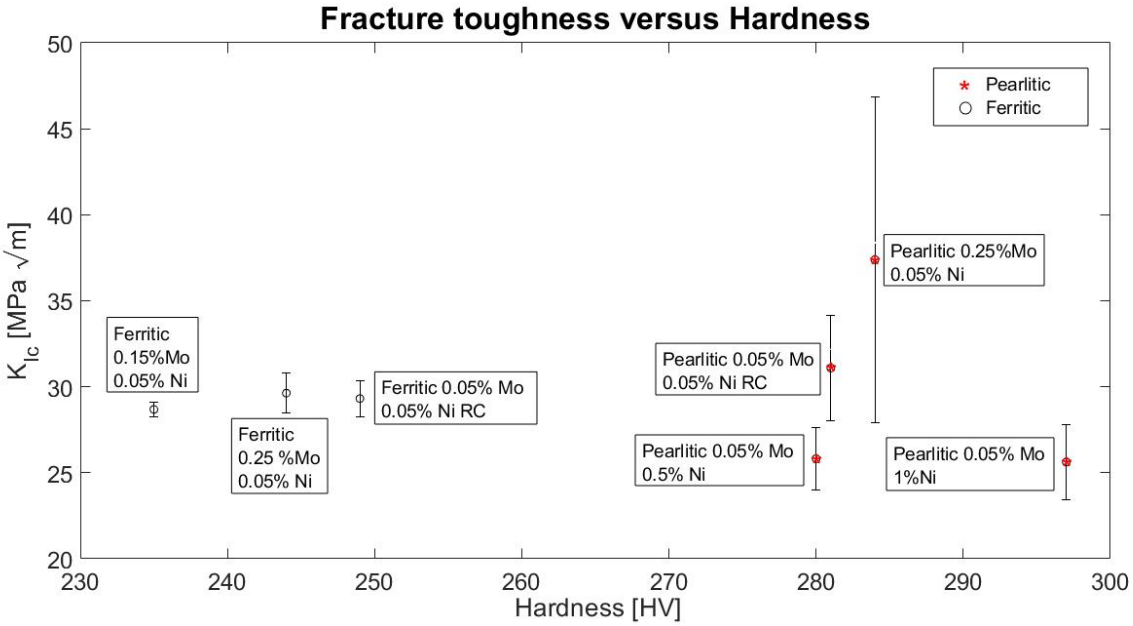

Figure 4.11: Relation between the fracture toughness and hardness values for the specimens tested.

4.3 Selection of the alloy with an advantageous performance

Deciding the proper alloy, in terms of the fracture toughness tests performance, is not as trivial as selecting the sample with the highest value. The analysis includes the correlation amongst the type of matrix, alloying elements quantities, fatigue crack growth rate performance, hardness, and graphite aspect ratio. In consideration of all the elements mentioned, it is possible to find within the alloys tested, the one with the most favourable performance for the cylinder head's requirements.

The type of matrix seems significantly to influence the fatigue crack growth rate. From the results related to the fatigue crack growth tests, it is possible to affirm that the pearlitic specimens tend to locate beneath the curves of the ferritic, denoting that the pearlitic alloys tend to display a slower fatigue crack growth rate. This last affirmation is sustained through the values of the Paris' law constants, C and m, where the samples with the lower m are the pearlitic specimens. The values of the fatigue crack growth rate at 17 $[MPa\sqrt{m}]$ also demonstrate this tendency, yet the difference within them is very little 6.2.

The hardness has a more significant influence on the fatigue crack growth rate in comparison with the aspect ratio. At the same time, the type of matrix seems to have a more relevant effect on the hardness, where the pearlitic specimens show to have the highest hardness and the lowest fatigue crack growth rate. The highest hardness of the pearlite matrix is associated with the ferrite and cementite layers, which it is compounded by. The lowest fatigue crack growth rate of the pearlitic specimens can be related to the fact that the crack needs to propagate through layers of cementite and ferrite, which display a higher crack growth resistance than a homogeneous matrix. This occurs for the specimens with a ferritic matrix. In conclusion, there is an evident influence of the type of matrix on the fatigue crack growth rate.

Furthermore, the considerable effect of the molybdenum on the graphite aspect ratio reduces its value for the pearlitic specimens. This element impact also decreases the pre-crack (stress concentration) effect of the graphite on the CGI.

From the results related to the fracture toughness test, it is possible to identify a substantial effect of the alloying elements on the fracture toughness, where the molybdenum, for the pearlitic specimens displays the highest fracture toughness value. Also, an evident influence of the nickel on the fracture toughness was identified displaying the lowest values. Although, the highest hardness was for the alloy with 1% Ni. This demeanor can be explained through the logic that the harder the alloy, the more brittle becomes.

For the rest of the alloys, the difference between the fracture toughness values was not relevant, thus no further conclusions were able to be made.

The alloying elements added in the ferritic specimens show nor clear influence on the performance of the fatigue crack growth rate, fracture toughness test, hardness, nor on the graphite aspect ratio. On the contrary, the pearlitic specimens display substantial influences of the molybdenum and nickel for quantities of 0.25% Mo and 1% Ni on the properties mentioned. The alloying elements in lower amounts showed an irrelevant effect.

The pearlitic specimen with 0.25% Mo displayed a slight hardening of the alloy in comparison with the pearlitic reference composition and 0.5% Ni samples. The effect of the nickel (only pearlitic specimens studied) showed a positive impact on the fatigue crack growth rate, the second with the lowest value. The graphitizing effect of the nickel displaying the highest hardness value of all the alloys tested, and the lowest fracture toughness value, was verified.

The fatigue crack growth and fracture toughness results obtained were compared with the ones reported in the research paper "Fracture Toughness and Crack Growth Rate of ferritic and pearlitic Compacted graphite irons at 25°C and 150°C" [7]. According to the Paris' law comparison, it was identified that the values obtained of the fatigue crack growth rate test are similar to the ones for samples with a vermicularity of 10-50 %. Although, the values reported of the ferritic specimens displayed lower values of the m constant. On the contrary, for the test performed in this current research, the lowest m values were attained with the pearlitic samples, which are related to a better fatigue crack growth curve demeanor.

The values reported of fracture toughness for specimens with a vermicularity of 10-50 % were within the range of 69.6 to 47.8 $[MPa\sqrt{m}]$, where the pearlitic specimens displayed higher values, in comparison to the ferritic ones. However, the fracture toughness values of this research were between 37.39 to 25.62 $[MPa\sqrt{m}]$, which coincides with a vermicularity within 90 % to a flake graphite morphology. Therefore, they are considerably below the ones reported. Although, the pearlitic specimens showed a higher fracture toughness for the values informed and the ones obtained with the tests performed. The difference between the values reported and the ones of the current research might be due to several factors, such as data acquisition technology, test parameters, and conditions. It is essential to understand that this document was written when technology was beginning to unravel.

Within "On the correlation between microstructural parameters and the thermo-mechanical fatigue performance of cast iron" [11] research, the graphite aspect ratio values for compacted graphite irons (ferritic, pearlitic, and ferritic-pearlitic matrices) were amidst the range of 4.12 to 4.94 [-]. The graphite aspect ratio for the alloys analyzed in this research (attained from the report "The casting procedure's impact on the microstructure" [38]) confirms that the specimens tested correspond to compacted graphite irons since their aspect ratio values were within the range of 4.02-5.08[.], which is quite similar to the ones informed.

Concerning the effect of the temperature on the fracture toughness (until 200°C), it was ob-

served a decrease not greater than 4 $[MPa\sqrt{m}]$. Therefore, it can be stated that the alloying elements and type of matrix have a larger influence on the fracture toughness than the temperature.

A qualitative analysis of the influences of the type of matrix and alloying elements on the fatigue crack growth rate, fracture toughness, aspect ratio, and hardness is displayed in the table 4.6. According to the numbers designated, it was likely to identify whether there is a major influence (number 2) or a regular one (number 1). For the fatigue crack growth rate and hardness, the most influential factor was the type of matrix. On the contrary, for the fracture toughness and aspect ratio, the alloying elements were the ones generating a bigger impact on these properties values. As it was mentioned, the effect of the type of matrix on the fracture toughness values was undetermined since no large differences between them were identified. Relating to the hardness, only the nickel had a relevant impact. Having said that, the matrix type has four points, and the alloy elements six points considered the evaluating scale. Therefore, the alloying elements have a more significant effect on the properties analyzed.

Property	Type of matrix	Alloying elements
Fatigue crack growth rate	2	1
Fracture toughness	undetermined	2
Aspect ratio	undetermined	2
Hardness	2	1
Total	4	6

Table 4.6: Degree of influence of the type of matrix and alloying elements on the properties analized.

- Degree 1: it has an influence on the property.
- Degree 2: it is the major influence on the property.

In recognition of all the results obtained, the alloy that best accomplishes the requirements for the cylinder heads corresponds to the pearlitic sample with 0.25% Mo. This composition displays a favourable combination of properties, which has the lowest m of the Paris' law constants (3.88 [-]), meaning a slight slope for the fatigue crack growth rate test. Other than, this contains a graphite morphology that concentrates less stress than the rest of the alloys. Consequently, it has the lowest graphite aspect ratio (4.02[-]). The fracture toughness performance of the pearlite 0.25% Mo specimen had the highest value, 37.39 $[MPa\sqrt{m}]$, which was 7.74 $[MPa\sqrt{m}]$ above the average from the samples tested.

Chapter 5

Conclusions

The chemical composition and the microstructure have a large impact on the mechanical properties of the alloy displayed. According to this research, the fatigue crack growth rate and fracture toughness are relevant properties to be analyzed for the cylinder head's material.

From the results obtained, there is an evident influence of the matrix on the fatigue crack growth rate and hardness. The pearlitic specimens showed a better performance in both of these properties. The decrease in the fatigue crack growth rate occurs due to the cementite and ferrite layers, which enhances the crack propagation resistance. The hardness increase is attributed to the combination of cementite and ferrite layers, which the pearlitic matrix is compound. The cementite contains a high amount of carbon, generating a greater deformation of the lattice structure leading to a higher hardness.

The effect of the alloying elements was observed on the graphite aspect ratio and substantially on the fracture toughness values. The molybdenum has a graphite refinement effect that not only generates graphite with a lower aspect ratio, but lessens the pearlitic inter-layers space as well. Consequently, the graphite and matrix concentrate less stress. Therefore, the pearlitic specimen with 0.25% Mo displayed the lowest aspect ratio, and the highest fracture toughness value. The specimens with nickel demonstrated the graphitizing effect of this element showing the highest hardness and the lowest fracture toughness value.

A comparison amidst the fatigue crack growth rate, fracture toughness, and aspect ratio with values reported in the literature review was performed. The Paris' law constants C and m (from the fatigue crack growth rate linear region of the curve) were within the range for specimens with a vermicularity of 10-50%. On the contrary, the fracture toughness values were similar to the ones with a vermicularity of 90% to a flake graphite morphology, according to the values informed [7]. The aspect ratio values were within the range for compacted graphite iron corresponding to the values reported [11].

From the results can be stated, that the combination of a ductile matrix, such as the ferritic

one, with the effect of the alloying elements, does not improve the alloy in terms of fracture toughness and fatigue crack growth rate test performance. On the opposite, the pearlitic matrix, compound by cementite and ferrite layers, offers suitable conditions of fatigue resistance, fracture toughness, graphite aspect ratio, and hardness. The pearlite matrix makes the action of the alloying elements possible, such as molybdenum and nickel allowing the carbon diffusion along the graphite surroundings. For the ferritic matrix, this last phenomenon was not possible. Thus there was no significant influence of the alloying elements.

In consideration of all the analyses performed, it is possible to confirm a significant and positive effect of the molybdenum at a concentration of 0.25% for the pearlitic specimens, displaying the lowest fatigue crack growth rate at 17 $[MPa\sqrt{m}]$, the lowest m Paris' law constant value (3.88 [-]), the highest fracture toughness (37.39 $[MPa\sqrt{m}]$) and the lowest aspect ratio (4.02[-]) of all the alloys tested. Therefore, the pearlitic alloy with 0.25% Mo is selected as the most suitable one for the cylinder heads' performance.

It is reasonable to continue the work to find the alloy that suits best the cylinder heads' service conditions. From the finishing line of this research, might be interesting and relevant to analyze the effect of adding bigger quantities of molybdenum in pearlitic alloys, up until 1% since it was proven to enhance relevant properties for the cylinder heads. Another aspect to consider for deeper research is to analyze samples with lower vermicularity including spheroidal graphite irons, which can be expected to display more favourable fatigue crack growth rate curves and higher fracture toughness values. Lastly, a cautious fracture analysis with an optical microscope could be made, to identify the crack growth demeanor across the microstructure of the specimens.

Chapter 6

Annexes

Specimen	C	Si	Mn (low)	P	Mo	Ni	Cr (low)	Sn (low)	Cu (low)
1MM	3.65	2.30	0.20	0.03	0.05	0.05	0.05	1.00	1.00
4MM	3.65	2.30	0.20	0.03	0.25	0.05	0.05	1.00	1.00
10MM	3.65	2.30	0.20	0.03	0.05	0.50	0.05	1.00	1.00
16MM	3.65	2.30	0.20	0.03	0.05	1.00	0.05	1.00	1.00
20MM	3.22	4.00	0.20	0.03	0.05	0.05	0.01	0.01	0.02
26MM	3.22	4.00	0.20	0.03	0.15	0.05	0.01	0.01	0.02
36MM (low)	3.22	4.00	0.20	0.03	0.25	0.05	0.01	0.01	0.02

Table 6.1: Table with specimens denotation and detailed percentage chemical composition from the data reported in the research [39]).

Matrix	Denotation	Composition			$\left(\frac{da}{dN}\right)$ [m/cycle]
		%Mo	%Ni	%Si	
Perlitic	1MM RC	0.05	0.05	2.30	$8.18 \cdot 10^{-8}$
	4MM	0.25	0.05		$4.86 \cdot 10^{-8}$
	10MM	0.05	0.50		$7.09 \cdot 10^{-8}$
	16MM	0.05	1.00		$6.97 \cdot 10^{-8}$
Ferritic	20MM RC	0.05	0.05	4.00	$9.85 \cdot 10^{-8}$
	26MM	0.15	0.05		$1.04 \cdot 10^{-7}$
	36MM	0.25	0.05		$9.58 \cdot 10^{-8}$

Table 6.2: Values of fatigue crack growth rate at 17 MPa$\sqrt{m}$ of stress intensity factor range obtained from the linear relation (Paris' law) between 15-18 MPa$\sqrt{m}$.

[1]

[1]RC: 0.05% Mo 0.05% Ni

Matrix	Denotation	Composition			Hardness [HV]
		%Mo	%Ni	%Si	
Perlitic	1MM	0.05	0.05	2.30	281 ± 8.36
	4MM	0.25	0.05		284 ± 8.47
	10MM	0.05	0.50		280 ± 5.64
	16MM	0.05	1.00		297 ± 4.89
Ferritic	20MM	0.05	0.05	4.00	249 ± 1.19
	26MM	0.15	0.05		235 ± 4.82
	36MM	0.25	0.05		244 ± 2.14

Table 6.3: Hardness values, denotation, composition and type of matrix for the specimens analysed in this document.

Bibliography

[1] A. butler. (2019). "Why does an engine have a cylinder head?", [Online]. Available: https://www.autobutler.co.uk/wiki/cylinder-head-functions-repairs (visited on 05/11/2019).

[2] Mechanicalenotes. (). "Major parts of an ic engine with their functions", [Online]. Available: https://mechanicalenotes.com/parts-of-ic-engine-with-its-function/ (visited on 08/25/2021).

[3] M. Béranger, G. Morin, S. Saanouni, A. Koster, and V. Maurel, "Fatigue of automotive engine cylinder heads – a new model based on crack propagation", *MATEC Web of Conferences*, vol. 165, p. 10 013, Jan. 2018. DOI: 10.1051/matecconf/201816510013.

[4] M. Benedetti, V. Fontanari, and D. Lusuardi, "Effect of graphite morphology on the fatigue and fracture resistance of ferritic ductile cast iron", *Engineering Fracture Mechanics*, vol. 206, pp. 427–441, 2019.

[5] B. auto parts. (2020). "What is a cylinder head?", [Online]. Available: https://www.buyautoparts.com/howto/what_is_a_cylinder_head.htm (visited on 05/13/2019).

[6] E. Guzik and S. Dzik, "A r c h i v e s structure and mechanical properties of vermicular cast iron in cylinder head casting", *Archives of Foundry Engineering*, vol. 9, Jan. 2009.

[7] Y.-B. C. Shen-Chih Lee, "Fracture toughness and crack growth rate of ferritic and pearlitic compacted graphite irons at 25°c and 150°c", *Metallurgical transactions A*, vol. 2A, pp. 2645–2653, Nov. 1991.

[8] S. Dawson, "Compacted graphite iron: Compacted graphite iron - a material solution for modern diesel engine cylinder blocks", vol. 185, pp. 170–172, Jun. 2011.

[9] sweden.se. (2020). "Saving the climate", [Online]. Available: https://sweden.se/climate/ (visited on 05/14/2019).

[10] M. Costa and D. Piazzullo, "Biofuel powering of internal combustion engines: Production routes, effect on performance and cfd modeling of combustion", *Frontiers in Mechanical Engineering*, vol. 4, p. 9, Aug. 2018. DOI: 10.3389/fmech.2018.00009.

[11] E. Kihlberg, V. Norman, P. Skoglund, P. Schmidt, and J. Moverare, "On the correlation between microstructural parameters and the thermo-mechanical fatigue performance of cast iron", *International Journal of Fatigue*, vol. 145, p. 106 112, 2021.

[12] E. ASTM, "Standard terminology relating to methods of mechanical testing", 2002.

[13] S. Estay, "Fundiciones grises", *Curso de Metalugia Física II*, 2018.

[14] ASTM, "Standard method for measurement of fatigue crack growth rates", *Anual book of ASTM standards*, 2014.

[15] I. ASTM, "Standard test methods for plane-strain fracture toughness and strain energy release rate of plastic materials", *ASTM D5045-99*, 2007.

[16] A. Lavakumar, *Concepts in Physical Metallurgy*, ser. 2053-2571. Morgan Claypool Publishers, 2017, ISBN: 978-1-6817-4473-5. DOI: 10.1088/978-1-6817-4473-5. [Online]. Available: https://dx.doi.org/10.1088/978-1-6817-4473-5.

[17] T. Materia. (2001). "Classification of cast iron", [Online]. Available: http://www.totalmateria.com/articles/Art63.htm (visited on 05/17/2019).

[18] ——, (2009). "Vermicular graphite cast iron", [Online]. Available: https://www.totalmateria.com/page.aspx?ID=CheckArticle&site=kts&NM=263 (visited on 05/17/2019).

[19] W. D. Callister Jr and D. G. Rethwisch, *Fundamentals of materials science and engineering: an integrated approach*. John Wiley & Sons, 2020.

[20] H. Boyer, "Fatigue testing", *Report of ASM International, USA*, 1986.

[21] Y. Cai and H. Sun, *Solutions for Biot's Poroelastic Theory in Key Engineering Fields: Theory and Applications*. May 2017, pp. 1–177. DOI: 10.1016/C2015-0-04262-9.

[22] M. Cyclopedia. (2016). "Material fatigue", [Online]. Available: https://www.comsol.com/multiphysics/material-fatigue (visited on 05/11/2019).

[23] P. Moore and G. Booth, "6. structures under cyclic load", in. Dec. 2015, ISBN: 9781782423706. DOI: 10.1533/9781782423911.1.65.

[24] Z. Ahmad, "Principles of corrosion engineering and corrosion control", *Principles of Corrosion Engineering and Corrosion Control*, Jan. 2006. DOI: 10.1016/B978-0-7506-5924-6.X5000-4.

[25] E. Hearn, "Chapter 11 - fatigue, creep and fracture", in *Mechanics of Materials 2 (Third Edition)*, E. Hearn, Ed., Third Edition, Oxford: Butterworth-Heinemann, 1997, pp. 443–508, ISBN: 978-0-7506-3266-9. DOI: https://doi.org/10.1016/B978-075063266-9/50012-3. [Online]. Available: https://www.sciencedirect.com/science/article/pii/B9780750632669500123.

[26] R. W. Hertzberg, R. P. Vinci, and J. L. Hertzberg, *Deformation and fracture mechanics of engineering materials*. John Wiley & Sons, 2020.

[27] H. Yang, M. Krause, and J. Renner, "Determination of fracture toughness of mode i fractures from three-point bending tests at elevated confining pressures", *Rock Mechanics and Rock Engineering*, vol. 54, no. 10, pp. 5295–5317, 2021.

[28] Wikipedia contributors, *Fracture mechanics — Wikipedia, the free encyclopedia*, [Online; accessed 7-March-2022], 2022. [Online]. Available: `https://en.wikipedia.org/w/index.php?title=Fracture_mechanics&oldid=1063944456`.

[29] J. Donoso, "Apuntes mecánica de fractura, parte 4", 2021.

[30] Wikipedia contributors, *Crack closure — Wikipedia, the free encyclopedia*, [Online; accessed 7-March-2022], 2020. [Online]. Available: `https://en.wikipedia.org/w/index.php?title=Crack_closure&oldid=994657612`.

[31] J. Donoso, "Apuntes mecánica de fractura, parte 10", 2021.

[32] R. peng, "Fatigue crack propagation, lecture 13", *Deformation and fracture*, 2019.

[33] D. Roylance, "Department of materials science and engineering massachusetts institute of technology cambridge, ma 02139 may 1, 2001", 2001.

[34] F. R. Morral, *Metalurgia general. Tomo 2*. Reverte, 2021, vol. 2.

[35] X.-R. Chen, Q.-J. Zhai, H. Dong, B.-H. Dai, and H. Mohrbacher, "Molybdenum alloying in cast iron and steel", *Advances in Manufacturing*, vol. 8, no. 1, pp. 3–14, 2020.

[36] E. P. DeGarmo, J. T. Black, and R. A. Kohser, *Materiales y procesos de fabricación*. Reverté, 1988, vol. 1.

[37] ASTM. (). "Astm about us", [Online]. Available: `https://www.astm.org/ABOUT/overview.html` (visited on 08/25/2021).

[38] E. N. Alfred Boman Hanna Jybrink, "The casting procedure's impact on the microstructure", *Linköpings universitet*, 2020.

[39] J. W. Jonathan Ahlsén Herman Titus, "The importance of the microstructure for the mechanical properties of compact graphite iron", *Linköpings universitet*, 2020.

[40] H.-y. Yang and M. Pan, "Engineering research in fluid power: A review", *Journal of Zhejiang University SCIENCE A*, vol. 16, pp. 427–442, Jun. 2015. DOI: `10.1631/jzus.A1500042`.

[41] M. Bionix, "Tabletop test systems", *mts.com*, 2017.

[42] T. Materia. (2001). "Cast irons", [Online]. Available: `https://www.totalmateria.com/page.aspx?ID=CheckArticle&site=kts&LN=EN&NM=20` (visited on 05/31/2022).

[43] F. de CCOO. de andalucia, "Metalografía", *revista digital para profesionales de la enseñanza*, 2011.